eLife

Reviewed Preprint
v1 • July 17, 2024
Not revised

Cancer Biology

Repression of PRMT activities sensitize homologous recombination-proficient ovarian and breast cancer cells to PARP inhibitor treatment

Youyou Zhang, Mu Xu, Jiao Yuan, Zhongyi Hu, Junjie Jiang, Jie Huang, Bingwei Wang, Jianfeng Shen, Meixiao Long, Yi Fan, Kathleen T Montone, Janos L Tanyi, Omid Tavana, Ho Man Chan, Xiaowen Hu, Lin Zhang

Center for Research on Reproduction & Women's Health, University of Pennsylvania, Philadelphia, Pennsylvania, 19104, USA • Department of Obstetrics and Gynecology, University of Pennsylvania, Philadelphia, Pennsylvania, 19104, USA • Abramson Cancer Center, University of Pennsylvania, Philadelphia, Pennsylvania, 19104, USA • Division of Hematology, Department of Internal Medicine, Ohio State University, Columbus, Ohio, 43210, USA • Department of Radiation Oncology, University of Pennsylvania, Philadelphia, Pennsylvania, 19104, USA • Department of Pathology and Laboratory Medicine, University of Pennsylvania, Philadelphia, Pennsylvania, 19104, USA • Center for Gynecologic Cancer Immunotherapies, University of Pennsylvania, Philadelphia, Pennsylvania, 19104, USA • Bioscience, Research and Early Development, Oncology R&D, AstraZeneca, Waltham, Massachusetts, 02451, USA

Abstract

An "induced PARP inhibitor (PARPi) sensitivity by epigenetic modulation" strategy is being evaluated in the clinic to sensitize homologous recombination (HR)-proficient tumors to PARPi treatments. To expand its clinical applications and identify more efficient combinations, we performed a drug screen by combining PARPi with 74 well-characterized epigenetic modulators that target five major classes of epigenetic enzymes. Both type I PRMT inhibitor and PRMT5 inhibitor exhibit high combination and clinical priority scores in our screen. PRMT inhibition significantly enhances PARPi treatment-induced DNA damage in HR-proficient ovarian and breast cancer cells. Mechanistically, PRMTs maintain the expression of genes associated with DNA damage repair and BRCAness and regulate intrinsic innate immune pathways in cancer cells. Analyzing large-scale genomic and functional profiles from TCGA and DepMap further confirms that PRMT1, PRMT4, and PRMT5 are potential therapeutic targets in oncology. Finally, PRMT1 and PRMT5 inhibition act synergistically to enhance PARPi sensitivity. Our studies provide a strong rationale for the clinical application of a combination of PRMT and PARP inhibitors in patients with HR-proficient ovarian or breast cancer.

eLife assessment

This study presents a **valuable** finding that PRMT inhibitors may exert synergistic effects with PARP inhibitors to eliminate ovarian and triple-negative cancer cells in vitro and in vivo using preclinical mouse models. The evidence supporting the claims of the authors is **solid**, although the inclusion of novelty justification would have strengthened the study. The work will be of interest to scientists working on breast cancer and ovarian cancer.

https://doi.org/10.7554/eLife.99225.1.sa2

Introduction

High-grade serous ovarian cancer (HGSOC) and triple-negative breast cancer (TNBC) share clinical and genomic characteristics, such as poor prognosis, homologous recombination (HR) deficiencies and potential immunoreactivity[1–4]. There is an urgent unmet medical need to develop effective therapeutic strategies for these two diseases. Recently, limited targeted-therapy options, such as the Poly (ADP-ribose) polymerase inhibitors (PARPis), have been approved to treat HGSOC and TNBC in a frontline setting as maintenance therapies or in a recurrent/metastatic setting[5–10]. However, the greatest clinical benefit from PARPi monotherapy has been mainly observed in HR-deficient tumors[5–10], only representing a minority of patients (less than 50% of patients even in HGSOC[1, 3]). Due to frequent defection of one or more DNA damage repair (DDR) pathways, increased replication stress, and higher endogenous DNA damage levels, cancer cells highly rely on the DDR pathways for survival compared with normal cells[10–14]. During tumorigenesis, to solve these crises, certain DDR-related genes are pathologically upregulated in cancer cells. Epigenetic mechanisms represent a major strategy used by cancer cells to maintain or restore their abnormal need for DDR gene expression, resulting in a targetable vulnerability (**Figure 1A**). This “Achilles’ heel” can be targeted by epigenetic modulators (e.g., BETi[15–17], CDK7/12i[18–20], DNMTi[21–23], and HDACi[24, 25]) or small molecules that indirectly modulate DDR gene transcription (e.g., PI3KCAi[26–29], AKTi[30, 31], mTORi[32], and MEKi[33], **Figure 1B**). Several groups, including our own[15], have developed an “induced PARPi sensitivity by epigenetic modulation” strategy[9, 10, 15] to preferentially impair the transcription of certain DDR genes, thereby sensitizing PARPi intrinsic and acquired resistant tumors to PARPi treatment. For example, our previous discovery on the combination of BETi and PARPi[15] is being evaluated in a Phase 1b/2 trial and achieving promising clinical results (NCT03901469)[34]. Excitingly, due to cancer cells being extremely sensitive to the epigenetic repression of DDR genes compared with normal cells, a therapeutic window for these combinations has been observed during early clinical development[23, 28–31, 34]. Although promising results have been reported in the clinic, the following two key questions still need to be addressed: First, among the clinically applicable epigenetic modulators, which epi-drug(s) can provide the strongest synergistic effects with PARPi? Second, can a BRCA-independent strategy be developed, given that most current strategies are mediated by repressing the expression of BRCA, which has been genomically mutated in acquired HR-proficient HGSOC/TNBC patients. Therefore, a highly effective and BRCA-independent strategy needs to be designed and evaluated.

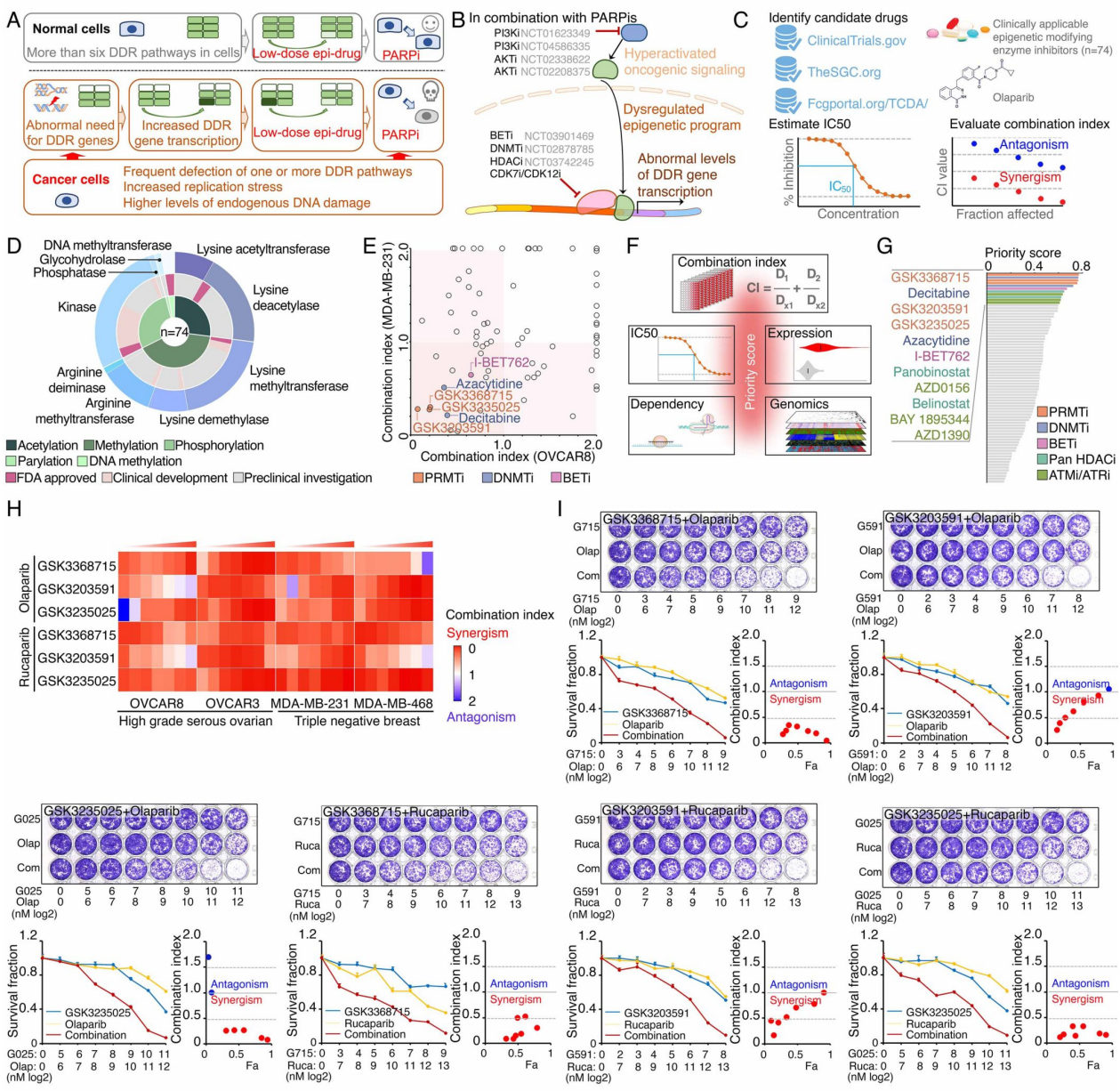
A
Normal cells
More than six DDR pathways in cells
Low-dose epi-drug
PARPi
Abnormal need for DDR genes
Increased DDR gene transcription
Low-dose epi-drug
PARPi
Cancer cells
Frequent defection of one or more DDR pathways
Increased replication stress
Higher levels of endogenous DNA damage
B
In combination with PARPis
PI3Ki NCT01623349
PI3Ki NCT04586335
AKTi NCT02338622
AKTi NCT02208375
Hyperactivated oncogenic signaling
Dysregulated epigenetic program
BETi NCT03901469
DNMTi NCT02878785
HDACi NCT03742245
CDK7i/CDK12i
Abnormal levels of DDR gene transcription
C
Identify candidate drugs
ClinicalTrials.gov
TheSGC.org
Fcgportal.org/TCDA/
Clinically applicable epigenetic modifying enzyme inhibitors (n=74)
Olaparib
Estimate IC50
% Inhibition
IC50
Concentration
Evaluate combination index
CI value
Antagonism
Synergism
Fraction affected
D
DNA methyltransferase
Glycohydrolase
Phosphatase
Lysine acetyltransferase
Kinase
Lysine deacetylase
n=74
Arginine deiminase
Lysine methyltransferase
Arginine methyltransferase
Lysine demethylase
Acetylation
Methylation
Phosphorylation
Parylation
DNA methylation
FDA approved
Clinical development
Preclinical investigation
E
Combination index (MDA-MB-231)
Combination index (OVCAR8)
I-BET762
Azacytidine
GSK3368715
GSK3235025
Decitabine
GSK3203591
PRMTi
DNMTi
BETi
F
Combination index
IC50
Expression
Dependency
Genomics
Priority score
G
Priority score
GSK3368715
Decitabine
GSK3203591
GSK3235025
Azacytidine
I-BET762
Panobinostat
AZD0156
Belinostat
BAY 1895344
AZD1390
PRMTi
DNMTi
BETi
Pan HDACi
ATMi/ATRi
H
Olaparib
GSK3368715
GSK3203591
GSK3235025
Rucaparib
GSK3368715
GSK3203591
GSK3235025
Combination index
Synergism
Antagonism
OVCAR8
OVCAR3
MDA-MB-231
MDA-MB-468
High grade serous ovarian
Triple negative breast
I
GSK3368715+Olaparib
GSK3203591+Olaparib
GSK3235025+Olaparib
GSK3368715+Rucaparib
GSK3203591+Rucaparib
GSK3235025+Rucaparib
Survival fraction
Combination index
Antagonism
Synergism
Combination
Olaparib
Rucaparib
(nM log2)
Fa

Figure 1.

Identification of synergistic actions between PRMTis and PARPi using a drug combination screen

A. Illustration of the "induced PARPi sensitivity by epigenetic modulation" strategy for treatment of cancer patients with HR-proficient tumors. Due to frequent defection of one or more DDR pathways, increased replication stress, and higher endogenous DNA damage levels, cancer cells highly rely on the DDR pathways for survival compared with normal cells. During tumorigenesis, to solve these crises, certain DDR-related genes are pathologically upregulated in cancer cells. Epigenetic mechanisms represent a major strategy used by cancer cells to maintain or restore their abnormal need for DDR gene expression, resulting in a targetable vulnerability. This "Achilles' heel" can be targeted by epigenetic modulators. **B.** Examples of the clinical trials based on the "induced PARPi sensitivity by epigenetic modulation" strategy. The combinations of PARPis with the epi-drugs or small molecules that indirectly modulate DDR gene transcription were evaluated in the clinic. **C.** Illustration the drug combination screen approach used in this study. **D.** The 74 epigenetic modifying enzyme inhibitors in the panel that was used for the drug combination screen were classified based on their mechanisms of action and target developmental levels. **E.** The combination index (CI) values were generated from a drug combination screen between olaparib and each epigenetic inhibitor in OVCAR8 and MDA-MB-231 cell lines. The CI quantitatively depicts synergism (CI < 0.83), additive effect (CI = 0.83-1.2), and antagonism (CI > 1.2). **F.** Five weighted features were collected and used to estimate the priority scores. **G.** The epigenetic inhibitors were ranked based on their priority scores, and the top prioritized inhibitors are highlighted. Color indicates mechanism of action. **H.** The heatmap shows average CI values between PARPis (olaparib or rucaparib) and PRMTis (GSK3368715, GSK3235025, or GSK3203591) in OVCAR8, OVCAR3, MDA-MB-231, and MDA-MB-468 cell lines. Color (red, synergism; blue, antagonism) intensity (light to dark) indicates increasing average CI values for each combination. **I.** An example of the sensitivity of cancer cells to PARPi alone, PRMTi alone, and a PARPi and PRMTi combination. Only results from OVCAR8 cells are shown here. The results from other cell lines are provided in Figure S1. For each treatment, the upper panel shows crystal violet staining of a colony formation assay; the lower left panel shows a quantified survival fraction; and the lower right panel shows the CI values. Fa, fraction affected.

Protein arginine methyltransferases (PRMTs) have emerged as attractive therapeutic targets in oncology owing to their crucial functions during tumorigenesis[35–39]. Arginine methylation is a common post-translational modification of proteins, playing crucial functions in the regulation of transcription[40–43], splicing[44–51], DDR[43, 52–67], and immune responses[43, 68, 69]. By transferring a methyl group from S-adenosylmethionine, PRMTs catalyze the formation of arginine residues with monomethylarginine (MMA), asymmetrical dimethylarginine (aDMA), and symmetrical dimethylarginine (sDMA)[35–39]. Each such methylation state affects protein function and interactions with other proteins or nucleic acids in different ways, leading to distinct functional consequences. Based on catalytic activities, nine PRMTs in mammalians are divided into three groups. Type I (PRMT1/2/3/4/6/8) and type II (PRMT5/9) enzymes catalyze the formation of MMA as an intermediate before the establishment of aDMA and sDMA, respectively. PRMT7 is a type III enzyme that catalyzes only the formation of MMA. The activities of PRMT1 and PRMT5 are responsible for generating most cellular aDMA and sDMA, respectively; therefore, they serve as the major type I and type II enzymes in cells, respectively[37, 70]. Type I and II PRMTs share common substrates, with preferences for histones (such as H3R2 and H4R3)[71] and proteins with RG/RGG motifs (such as RNA-binding proteins and splicing complex proteins)[72]. This substrate overlaps and competitive behavior leads to the phenomenon of substrate scavenging[48, 73–75]. For example, PRMT1 and PRMT5 scavenge each other's substrates in cells[75].

Recently, potent and selective PRMT inhibitors (PRMTis) have been successfully developed, and more than ten PRMTis have been rapidly advanced into early clinical trials[35–39]. Although relatively rare genomic alterations in the genes encoding PRMTs are observed in cancer, expression levels of PRMTs are remarkably upregulated in solid tumors, and elevated PRMT expression is significantly associated with poor clinical outcome. Therefore, PRMTs have been

considered as attractive drug targets in oncology. Preclinical studies suggest that PRMT-targeting therapies may benefit tumors with MTAP deletion[73, 76–79] or splicing dysfunction[44–50, 80]. Although PRMTis provide a new avenue for cancer treatment, translational challenges need to be addressed for their clinical application. The PRMTi targetable "Achilles' heels" (MTAP deletion and splicing dysfunction) are only observed in a small fraction of cancers, which restricts the application of a PRMTi as a clinical monotherapy. Therefore, the development of a novel treatment strategy to expand the potential clinical applications is a key challenge for PRMTis in oncology. Most importantly, because recent clinical trial results indicated that PRMTi activity alone may be insufficient to manage patients[81–88], even in MTAP deletion setting, pharmaceutical companies have had to terminate these trials and "re-think" how to administer these drugs to patients. Therefore, combination approaches of low-dose PRMTi with other existing therapeutic drugs urgently need to be designed and evaluated in the clinic. Excitingly, recent studies have revealed promising synergistic effects between PRMTis and chemotherapy, as well as DDR targeting drugs[89–92].

Results

Identification of synergistic actions between PRMTis and PARPi using a drug combination screen

To expand clinical applications and identify more efficient combinations for the "induced PARPi sensitivity by epigenetic modulation" strategy, we performed a drug screen by combining PARPi with a set of epigenetic modifying enzyme inhibitors, which contain 74 well-characterized epigenetic modulators that target 5 major classes of epigenetic enzymatic actions, histone acetylation, histone methylation, histone phosphorylation (only kinases and phosphatases that modify histone were included), histone de-ADP-ribosylation, and DNA methylation. Among these inhibitors, 7 are FDA-approved drugs in oncology, and 14 and 54 are in clinical trials and preclinical development, respectively (**Figure 1C** and **1D** and Table S1). The BET inhibitor I-BET762, a previously identified epigenetic modulator that synergistically acts with PARPi[15], was used as a positive control. Two cancer cell lines that harbor wild type BRCA1/2 and modestly respond to PARPi (OVCAR8, HGSOC; and MDA-MB-231, TNBC) were used for screening. After the IC50s of each drug were estimated in these two lines, five gradient doses (serially constant two-fold ratio dilutions) were used for the drug combination screen. The combination index (CI) value of olaparib with each epigenetic inhibitor was calculated to evaluate the synergy of the combinations. In summary, synergistic effects with olaparib (medium CI value <0.83) were identified in 33 and 21 epigenetic inhibitors in OVCAR8 and MDA-MB-231, respectively, including 10 that were shared by the two lines (**Figure 1E** and Table S1). Next, to prioritize the clinical application potentials, we estimated a priority score for each combination by considering the CI and four additional features of each epigenetic inhibitor (single agent treatment efficacy, cancer dependency defined by genetic screen from the DepMap project, and expression dysregulation and genomic alterations from the TCGA project, **Figure 1F**). As expected, candidates previously identified by us[15] and other groups, such as BETi[15–17], DNMTi[21, 22], and HDACi[24, 25], were ranked at the top of the list (**Figure 1G** and Table S1). Notably, a group of PRMT inhibitors (type I PRMTs targeting GSK3368715, and PRMT5 targeting GSK3203591 and GSK3235025) exhibited high priority scores in our analysis. This observation was further confirmed in an expanded panel of HGSOC/TNBC cell lines that were treated with each of these PRMTis in combination with two FDA-approved PARPis, olaparib and rucaparib, independently (**Figure 1H**, 1I, and Figure S1).

PRMT1, PRMT4/CARM1, and PRMT5 are potential therapeutic targets in oncology

To comprehensively characterize PRMTs in cancers, we analyzed the expressions and genomic alterations of all the PRMT family members across the TCGA cohort from 33 cancer types (Table S2). An RNA-sequencing (RNA-seq) analysis indicated that although all the PRMT family members were detectable in cancers, five PRMTs (PRMT1/2/4/5/7) exhibited remarkably high expression levels (average FPKM >10, **Figure 2A**, Figure S2A and Table S3). We also characterized expressional differences between tumors and their corresponding normal adjacent tissues. A meta-analysis across 21 cancer types, which had sufficient numbers of normal controls ($n \geq 3$), revealed that the mRNA levels of most PRMTs, except for PRMT2/9, were significantly upregulated in tumor specimens compared with corresponding controls (**Figure 2B** and Figure S2B). This observation was further validated at protein levels in an independent sample cohort from the CPTAC project as assessed by a mass spectrometry analysis (**Figure 2C** and Figure S2C). Most importantly, a meta-analysis across 33 cancer types from the TCGA cohort demonstrated that higher expressional levels of PRMT1/3/4/5 were positively correlated with shorter patient survival times (**Figure 2D**). Next, we analyzed recurrent genomic alterations (focal somatic copy number alteration, recurrent mutation, and recurrent transcript fusion) of the PRMT family across the TCGA cohort, and no significantly recurrent events were identified at either the individual or pan cancer levels (Table S4). Finally, cancer cell-growth dependencies of PRMTs were analyzed in a large-scale CRISPR screening dataset generated by the DepMap project. Consistence with their increased expression levels and associations with poor clinical outcomes, PRMT1/4/5 showed cancer cell-growth dependencies (**Figure 2E** and Table S5). The analyses of these five features indicated that two type I PRMTs (PRMT1 and PRMT4/CARM1) and one type II PRMT (PRMT5) may serve as potential therapeutic targets in oncology (**Figure 2F**). Because a PRMT4-specific inhibitor, CARM1-IN-1, did not show significantly synergistic effects with PARPi (**Figure 1B** and Table S1), we hypothesized that the synergistic function of type 1 PRMT inhibitor GSK3368715 may be mediated by inhibiting PRMT1, which is the predominant enzyme among type I PRMTs (responsible for >90% activity)[70]. Consequently, we used CRISPR/Cas9 as a genetic tool to specifically knock out PRMT1 and PRMT5 independently in OVCAR8 and MDA-MB-231 cells (**Figure 2G** and **2H**). Colony formation assays demonstrated that an acute knock out of PRMT1 or PRMT5 significantly increased the sensitivity levels of cancer cells to PARPi treatment, thereby phenocopying the results obtained using chemical PRMT inhibitors (**Figure 2I** and **2J**).

PRMT inhibition enhances PARPi treatment-induced DNA damage in cancer cells

To determine whether PRMTis influence DNA damage responses induced by PARPi treatments, a comet assay was used to measure DNA damage in a panel of HR-proficient cancer cells that had been treated with olaparib alone or in combination with PRMTis. Although the olaparib treatment alone induced DNA damage in all four HR-proficient cancer cell lines, the extent of the DNA damage increased significantly when cells were treated with a combination of PRMTis (GSK3368715 or GSK3235025) and olaparib (**Figure 3A, B** and Figure S3A). This observation was further confirmed by a western blot assay to detect the DNA double-strand break marker, the phosphorylation of H2AX (γH2AX [S139]), among different treatment conditions (**Figure 3C**). Consistence with the enhanced DNA damage, the combination treatment significantly induced apoptosis, as measured by caspase-3/7 activity (**Figure 3D**), compared with the olaparib treatment alone. To exclude the potential off-target effects of PRMT chemical inhibitors, PRMT1 and PRMT5 were knocked out independently using CRISPR/Cas9 in OVCAR8 and MDA-MB-231 cells (**Figure 2G**). The specific knockout of PRMT1 or PRMT5 significantly enhanced the DNA damage induced by the PARPi treatment, thereby increasing apoptosis (**Figure 3E**–**3G** and Figure S3B). These observations suggested that the increased expressions of PRMT1 and PRMT5 in cancer may

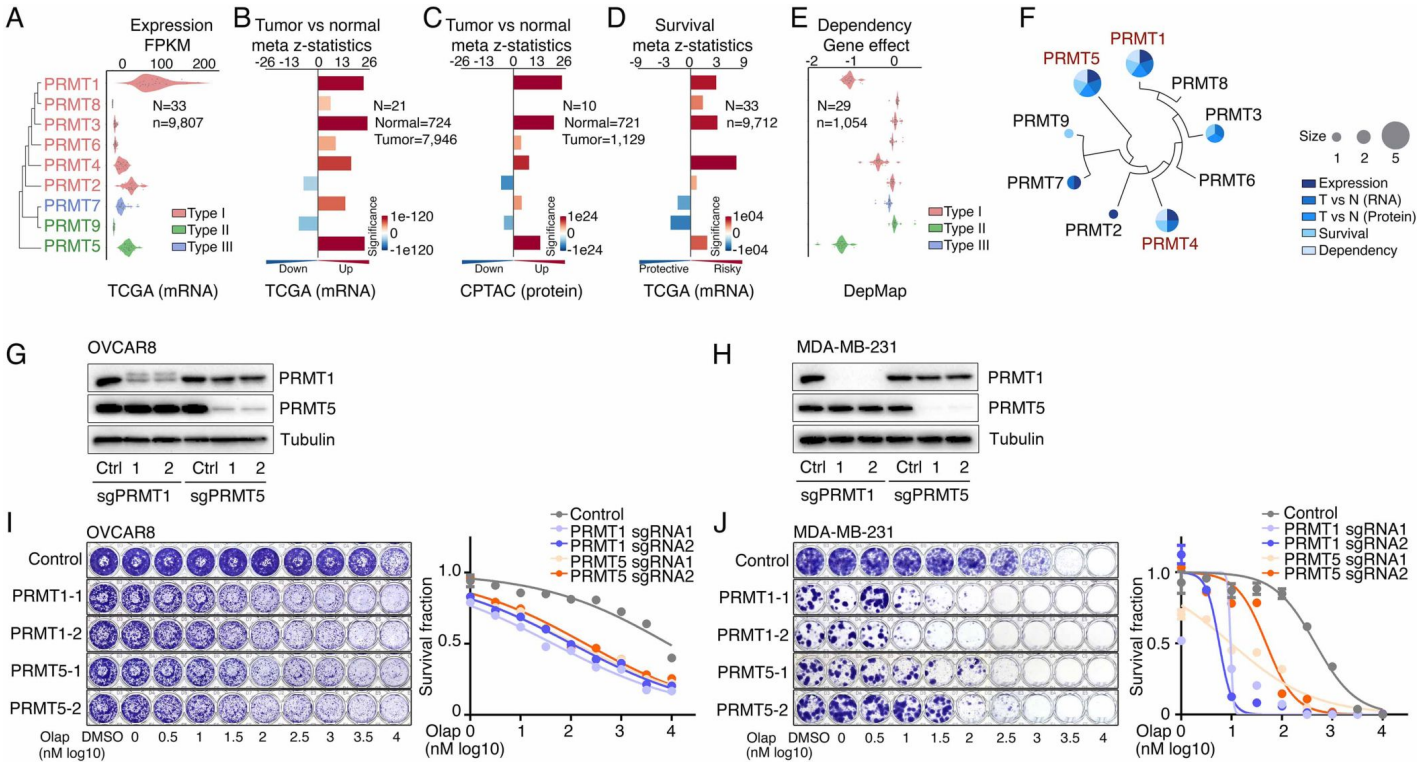

Figure 2.

PRMT1, PRMT4/CARM1, and PRMT5 are potential therapeutic targets in oncology

A. mRNA expression levels of the PRMT family across the TCGA tumor samples. Each spot represents the average mRNA expression level of a cancer type (n = 33). **B.** and **C.** Meta z-statistics of mRNA (B) and protein (C) expression levels of the PRMT family in tumors compared with corresponding controls in the TCGA (B) or CPTAC (C) cohorts. Red and blue indicate up-and down-regulation, respectively. **D.** Meta z-statistics of the association between mRNA expression and patient outcome for the PRMT family across the TCGA cohort. Red and blue indicate poor and good outcomes, respectively. **E.** The dependency effects of the PRMT family based on the CRISPR screen from the DepMap project. Each spot represents the average gene effect of a cancer type (n = 29). A lower effect score indicates that a gene is more likely to be dependent in cancer cells. **F.** Summary of the above five features for each gene in the PRMT family. **G.** and **H.** Western blot analyses of PRMT1 and PRMT5 expression in OVCAR8 (G) and MDA-MB-231 (H) cells in which PRMT1 and PRMT5 were independently knocked out using lentiviral CRISPR/Cas9. **I.** and **J.** Sensitivity of olaparib in OVCAR8 (I) or MDA-MB-231 (J) cells in which PRMT1 and PRMT5 were independently knocked out using lentiviral CRISPR/Cas9. Left panel: crystal violet staining of a colony formation assay; right panel: survival fraction quantified from the left panel.

prevent cell death by enhancing DNA damage repair when tumor cells are exposed to endogenous or exogenous DNA damage-causing conditions. Consequently, we analyzed the correlations between the expression levels of PRMT1/5 and "50 hallmark" molecular signatures[93] in a large collection of cancer cell lines from the DepMap project (n = 1,200). Consistently, "DNA-repair" was a significant signature that positively corrected with both PRMT1 and PRMT5 expression levels in cancer cell lines (**Figure 3H**). Similar results were found in the primary tumor specimens across the TCGA cohort at individual cancer type and pan cancer levels (**Figure 3I**, 3J and Table S6). Supporting previous reports that the Myc-PRMT loop plays critical roles during tumorigenesis, "Myc-targets" signatures were the most significant signatures correlated with the expression of PRMT1/5 (**Figure 3H–J**).

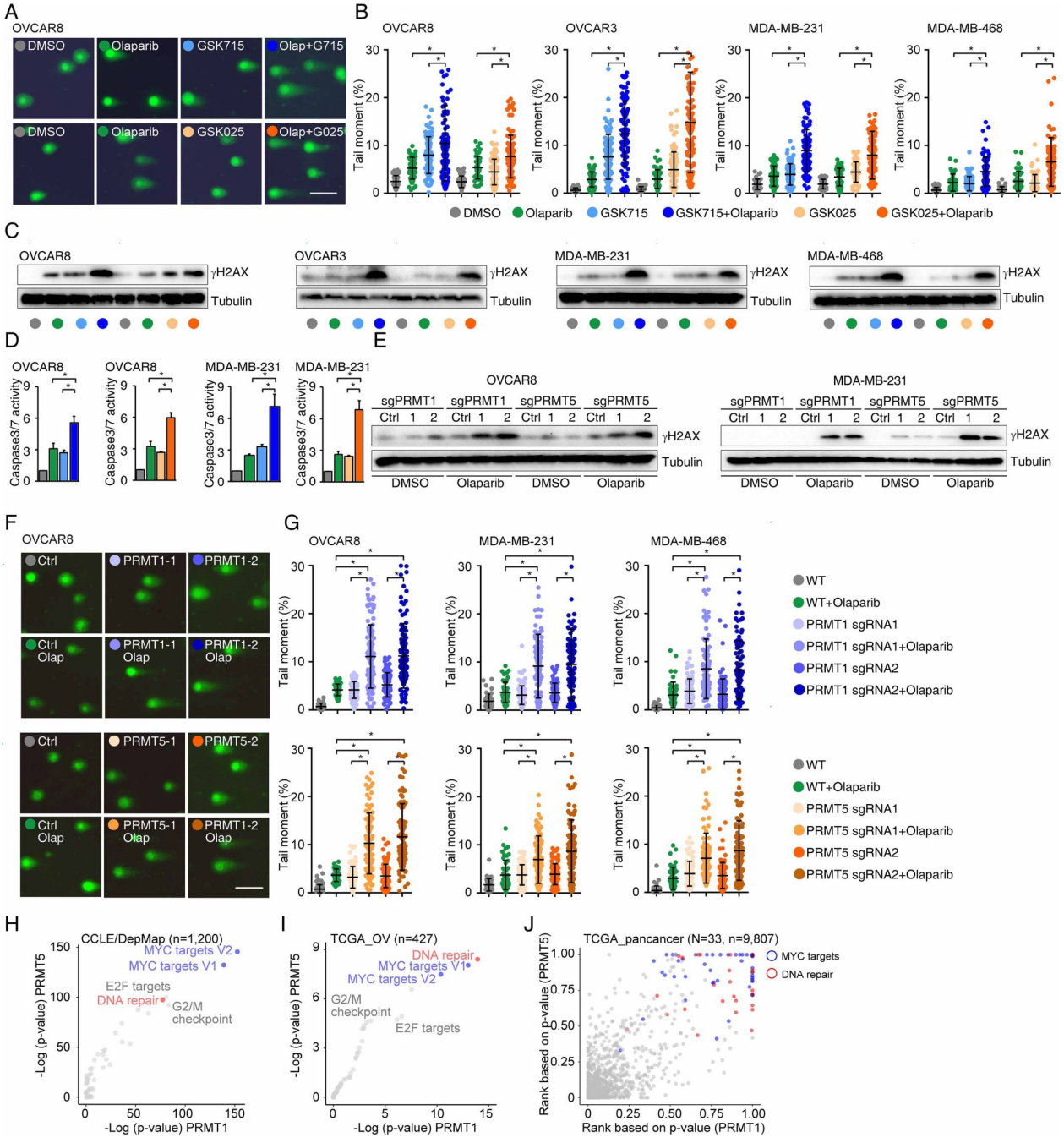
A
OVCAR8
DMSO
Olaparib
GSK715
Olap+G715
DMSO
Olaparib
GSK025
Olap+G025
B
OVCAR8
OVCAR3
MDA-MB-231
MDA-MB-468
Tail moment (%)
DMSO
Olaparib
GSK715
GSK715+Olaparib
GSK025
GSK025+Olaparib
C
OVCAR8
OVCAR3
MDA-MB-231
MDA-MB-468
γH2AX
Tubulin
D
OVCAR8
OVCAR8
MDA-MB-231
MDA-MB-231
Caspase3/7 activity
E
OVCAR8
MDA-MB-231
sgPRMT1
sgPRMT5
Ctrl
1
2
γH2AX
Tubulin
DMSO
Olaparib
F
OVCAR8
Ctrl
PRMT1-1
PRMT1-2
Ctrl Olap
PRMT1-1 Olap
PRMT1-2 Olap
Ctrl
PRMT5-1
PRMT5-2
Ctrl Olap
PRMT5-1 Olap
PRMT1-2 Olap
G
OVCAR8
MDA-MB-231
MDA-MB-468
Tail moment (%)
WT
WT+Olaparib
PRMT1 sgRNA1
PRMT1 sgRNA1+Olaparib
PRMT1 sgRNA2
PRMT1 sgRNA2+Olaparib
WT
WT+Olaparib
PRMT5 sgRNA1
PRMT5 sgRNA1+Olaparib
PRMT5 sgRNA2
PRMT5 sgRNA2+Olaparib
H
CCLE/DepMap (n=1,200)
MYC targets V2
MYC targets V1
E2F targets
DNA repair
G2/M checkpoint
-Log (p-value) PRMT5
-Log (p-value) PRMT1
I
TCGA_OV (n=427)
DNA repair
MYC targets V1
MYC targets V2
G2/M checkpoint
E2F targets
-Log (p-value) PRMT5
-Log (p-value) PRMT1
J
TCGA_pancancer (N=33, n=9,807)
MYC targets
DNA repair
Rank based on p-value (PRMT5)
Rank based on p-value (PRMT1)

Figure 3.

PRMT inhibition enhances PARPi treatment-induced DNA damage in cancer cells

A. A comet assay was used to measure DNA damage in cancer cells treated with DMSO, olaparib (5 μM, 96 h), GSK3368715 (5 μM, 96 h), GSK3235025 (5 μM, 96 h), or combinations (representative images from OVCAR8). Scale bars, 10 μm. **B.** The extent of DNA damage was quantified using the tail moment in comet assays of OVCAR8, OVCAR3, MDA-MB-231, and MDA-MB-468 cell lines treated with DMSO, olaparib, GSK3368715, GSK3235025, or combinations. Data are presented as means ± SDs, *p < 0.05 determined by two-tailed Student's t tests. **C.** Western blot analyses of γH2AX in cancer cells treated with DMSO, olaparib, GSK3368715, GSK3235025, or combinations. **D.** Caspase-3/7 activity was measured using a caspase-Glo 3/7 assay in OVCAR8 and MDA-MB-231 cells treated with DMSO, olaparib, GSK3368715, GSK3235025, or combinations. Data are presented as means ± SDs, n = 3 biological replicates, *p < 0.05 determined by two-tailed Student's t tests. **E.** Western blot analyses of γH2AX in OVCAR8 and MDA-MB-231 cells in which PRMT1 and PRMT5 were independently knocked out using lentiviral CRISPR/Cas9. **F.** A comet assay was used to measure olaparib treatment-induced DNA damage in cells in which PRMT1 and PRMT5 were independently knocked out using lentiviral CRISPR/Cas9 (representative images from OVCAR8). Scale bars, 10 μm. **G.** The extent of olaparib treatment-induced DNA damage was quantified using the tail moment in comet assays of OVCAR8, MDA-MB-231, and MDA-MB-468 cell lines in which PRMT1 and PRMT5 were independently knocked out using lentiviral CRISPR/Cas9. Data are presented as means ± SDs, *p < 0.05 determined by two-tailed Student's t tests. **H.** and **I.** Correlations between the expression levels of PRMT1/PRMT5 and "50 hallmark" molecular signatures in the cancer cell lines from the DepMap (H) and primary tumor specimens from the TCGA (ovarian cancer was represented as an example, I) cohort. **J.** Correlations between the expression levels of PRMT1/PRMT5 and "50 hallmark" molecular signatures across primary tumor specimens from the TCGA cohort. For each cancer type, the correlations between PRMT1/5 expression and "50 hallmark" molecular signatures were ranked 0 to 1 based on the p-values, with 1 indicating the most significant signature. Red and blue circles indicate DNA repair and Myc signatures, respectively.

PRMTs maintain expression of the genes associated with DDR and BRCAness

Given that PRMTs act as key epigenetic regulators through the modification of histone methylation, we investigated gene expression changes induced by PRMTi treatments. An RNA-seq analysis revealed that GSK3368715 and GSK3235025 treatments reduced protein-coding gene expression in MDA-MB-231 cells by approximately 12.7% and 6.9%, respectively (**Figure 4A**). Consistent with correlation analyses in cancer cell lines and primary tumors (**Figure 3H** to **3J**), a gene set enrichment analysis found that the downregulated genes in both the GSK3368715 and GSK3235025 treatment groups were significantly enriched in the DDR-associated pathways compared with controls (**Figure 4B**). The epigenetically repression of certain DDR genes induces the BRCAness phenotype, sensitizing cancer cells to PARPi treatments. Therefore, we collected the genes in the homologous recombination (HR) and Fanconi anemia (FA) pathways (two major DDR pathways affecting PARPi sensitivity)[94, 95], as well as the genes that were previously reported to be associated with PARPi sensitivity[96]. A total of 247 genes potentially implicated in PARP inhibitor sensitivity (i.e., BRCAness genes) were identified in a whole genome (**Figure 4C** and Table S7). As expected, many were downregulated by GSK3368715 (n = 29) and GSK3235025 (n = 31) treatments, with nine being significantly repressed by both of the PRMTis (**Figure 4A** and Table S8). This result was further validated by a qRT-PCR analysis (**Figure 4D**). Beyond epigenetic regulation, PRMTs play functional roles in RNA splicing through the methylation of RG/RGG motif-containing proteins in the splicing complexes. Consequently, we analyzed global RNA splicing changes between PRMTi treatments and controls. Consistent with previous reports, both the GSK3368715 and GSK3235025 treatments affected RNA splicing genome wide (**Figure 4E**). However, genes undergoing splicing changes were not significantly enriched in most DDR

pathways (except for base excision repair in the GSK3235025 treatment) (**Figure 4F**), although splicing alterations were identified in certain BRCAness genes, such as ERCC1, after PRMTi treatments (**Figure 4G**). Unexpectedly, we found that a PARPi treatment alone also induced modest but significant splicing alterations compared with the control (**Figure 4E**). Combination treatments with GSK3235025, but not GSK3368715, significantly further enhanced splicing alterations compared with an olaparib or GSK3235025 treatment alone (**Figure 4E**). Thus, both PRMT1i and PRMT5i treatments repressed mRNA expression of a large number of BRCAness genes in cancer cells. Although some genes were inhibited by both inhibitors, PRMT1i and PRMT5i repressed distinct BRCAness genes. Splicing alterations in certain BRCAness genes were identified after a PRMTi treatment, and the PARPi-treatment-induced splicing susceptibility may also serve as a mechanism for the synergistic action of PRMTi and PARPi.

Repression of ERCC1 is a common mechanism by which PRMTis sensitize cells to PARPi treatment

To evaluate whether the BRCAness genes, which were repressed by PRMTis, play functional roles in synergistic action between PRMTis and PARPi, a customer-designed siRNA screen was performed in MDA-MB-231 cells (**Figure 5A**), and an impact score for each candidate was estimated based on 1) expressional repression effects of PRMTis and 2) functional effects on PARPi sensitivity (**Figure 5B**). Among the candidates examined, ERCC1 had the highest impact score and was repressed by both GSK3368715 and GSK3235025 treatments (**Figure 5C**). In lung cancer, knocking out ERCC1 sensitizes cells to PARPi treatments[97], and its expression serves as a predictive biomarker for the platinum response[98]. Therefore, we used ERCC1 as an example to evaluate whether transcriptional repression can serve as a mechanism. We found that, similar to PRMTs, ERCC1 expression was significantly upregulated across cancer samples compared with their corresponding control specimens (**Figure 5D**). Consistent with the association between PRMT1/5 and the DDR signature (**Figure 3**), significant positive correlations between PRMT1/5 and ERCC1 mRNA expression levels were observed in primary tumor specimens from the TCGA cohort (**Figure 5E**). These results suggest that elevated PRMT expression in cancer may serve as a mechanism to epigenetically maintain ERCC1 expression, which is critical to the survival of cancer cells that are subjected to high levels of endogenous DNA damage and increased replication-related stress. Using western blots, we demonstrated that PRMTi treatments repressed ERCC1 expression at the protein level in a dose-dependent manner (**Figure 5F**). As expected, under these treatment conditions, GSK3368715 and GSK3235025 reduced global aDMA and sDMA levels, respectively. Notably, in consistence with previous reports[73], [99], the GSK3368715 treatment also increased global sDMA levels (Figure S4), suggesting that PRMT1 and PRMT5 share a substrate (i.e., MMA), and/or their functions may be compensatory in certain cellular contexts[73], [99]. These observations were also validated by genetically knocking out PRMT1 and PRMT5 independently using CRISPR/Cas9 (**Figure 5G** and Figure S4B). To determine whether the repression of ERCC1 by PRMTis was mediated by an epigenetic (transcriptional) mechanism, we cloned the ERCC1 promoter region (−1,500 to +120) and inserted it into a reporter vector (pGL3-basic). Both the chemical PRMTi treatment and genetic knockout of PRMT1/5 significantly reduced ERCC1 promoter activities in cells (**Figure 5H**). Next, we determined whether the PRMTi treatment was able to reduce the ERCC1 function. ERCC1 and XPF form a structure-specific nuclease that is required for the removal of ultraviolet (UV) radiation-generated cyclobutane pyrimidine dimers (CPDs). Thus, measuring the rate of UV-induced CPD removal serves as a semi-quantitative assay to monitor ERCC1 activity[100], [101] (**Figure 5I**). The OVCAR8 cells were pretreated with GSK3368715 (2.5 μM) and GSK3235025 (5 μM) independently for 48 h, then CPDs were induced by exposure to UV radiation (15 J/m^2, **Figure 5I**). Using a specific CPD antibody (Kamiya Biomedical Company, MC-062)[100], [101], immunofluorescent staining demonstrated that PRMTi treatments significantly decreased the CPD removal rates compared with controls after UV exposure (**Figure 5J**). This observation was validated by genetically knocking out PRMT1 or PRMT5 using CRISPR/Cas9 (**Figure 5K**). Additionally, a DNA-blotting assay confirmed the

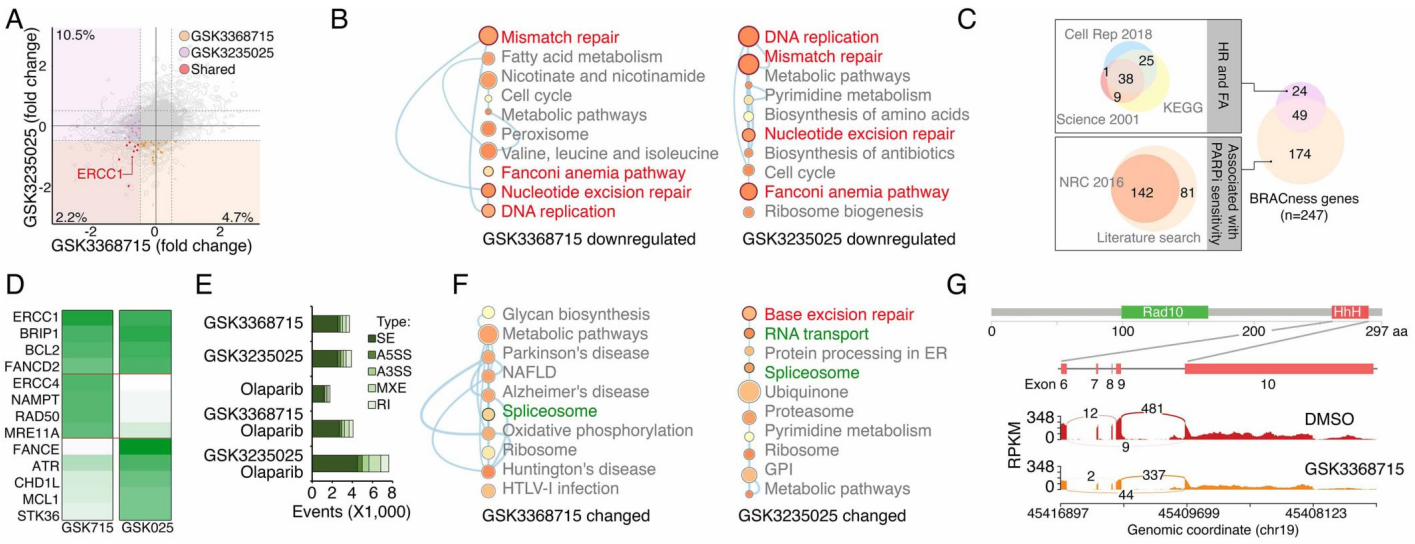

Figure 4.

PRMTis maintain the expression of genes associated with DNA damage repair (DDR) and BRCAness

A. The dot plot shows the gene expression changes measured by RNA-seq in MDA-MB-231 cells. The BRCAness genes that were repressed by GSK3368715 and GSK3235025 treatments are highlighted with color. **B.** The top 10 KEGG pathways in which genes downregulated by GSK3368715 (left) and GSK3235025 (right) treatments were significantly enriched. Circle size indicates the fold enrichment. Lines indicate numbers of shared genes between pathways. The DDR pathways are highlighted in red. **C.** Illustration BRCAness gene collection method. First, the genes in two major DDR pathways associated with PARPi sensitivity (HR and FA) were collected from three independent databases. In total, 73 genes annotated by at least two databases were defined as HR/FA genes. Second, the genes associated with PARPi sensitivity were retrieved from a Nature Reviews paper (n = 142). An additional 81 genes were identified through a manual literature search using PubMed. In total, 223 genes were defined as PARPi sensitivity-associated genes. Taken together, 247 genes were defined as “BRCAness genes” in this study. **D.** The heatmap shows qRT-PCR validation of a group of BRCAness genes. Color intensity indicates fold changes. Blue: downregulation, red: upregulation. **E.** The abnormal splicing event numbers induced by different treatments compared with the control treatment (DMSO) in MDA-MB-231 cells. Types of abnormal splicing events are indicated by different colors. **F.** The top 10 KEGG pathways in which abnormally spliced genes after GSK3368715 (left) and GSK3235025 (right) treatments were significantly enriched. Circle size indicates the fold enrichment. Lines indicate numbers of shared genes between two pathways. **G.** An abnormal splicing gene (ERCC1). Upper panel: the structure of ERCC1. The alternative splicing event was identified in exon 6-10, which encodes the helix-hairpin-helix (HhH) domain of ERCC1. Lower panel: Sashimi plots showing the exon truncation events of ERCC1 as detected by RNA-seq in MAD-MB-231 cells treated with DMSO and GSK3368715 independently. The X-axes indicate genomic locations, and the Y-axes indicate RNA-seq coverage. The numbers of junction reads are shown in the splice junctions (curved lines).

immunofluorescent staining results (**Figure 5L, M**). To further demonstrate the functional involvement of ERCC1 in the synergistic actions between PRMTis and PARPi, we knocked out ERCC1 in cancer cell lines using CRISPR/Cas9 (**Figure 5N**). As expected, the ERCC1-XPF activity was significantly reduced (Figure S5). Colony formation assays demonstrated that ERCC1 knockout cancer cell lines were sensitized to PARPi treatments (**Figure 5O**). Finally, the forced ERCC1 expression by lentiviral infection partially reduced the synergistic actions between PRMTis and PARPi in these cell lines (**Figure 5P**). Therefore, both type I PRMT and PRMT5 inhibitor treatments significantly repressed ERCC1 expression and activity levels in cancer cells. ERCC1 serves as a common mechanism by which PRMTis sensitizes cells to PARPi treatments.

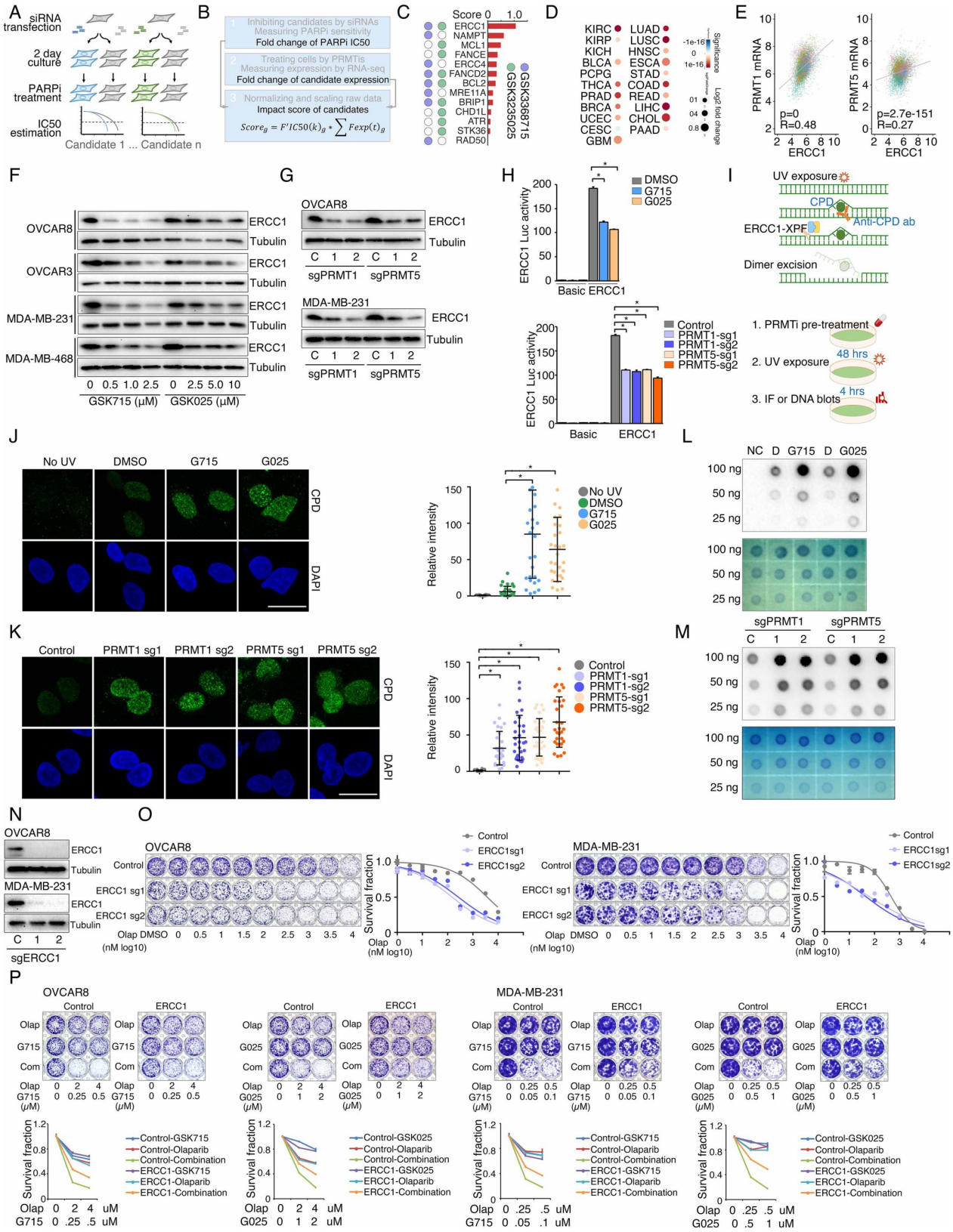
A
siRNA transfection
2 day culture
PARPi treatment
IC50 estimation
Candidate 1 ... Candidate n
B
1 Inhibiting candidates by siRNAs Measuring PARPi sensitivity
Fold change of PARPi IC50
2 Treating cells by PRMTis Measuring expression by RNA-seq
Fold change of candidate expression
3 Normalizing and scaling raw data
Impact score of candidates
C
Score 0 1.0
ERCC1
NAMPT
MCL1
FANCE
ERCC4
FANCD2
BCL2
MRE11A
BRIP1
CHD1L
ATR
STK36
RAD50
GSK3368715
GSK2335025
D
KIRC KIRP KICH BLCA PCPG THCA PRAD BRCA UCEC CESC GBM
LUAD LUSC HNSC ESCA STAD COAD READ LIHC CHOL PAAD
Log2 fold change
Significance
E
PRMT1 mRNA
PRMT5 mRNA
p=0
R=0.48
p=2.7e-151
R=0.27
ERCC1
F
OVCAR8
OVCAR3
MDA-MB-231
MDA-MB-468
ERCC1
Tubulin
0 0.5 1.0 2.5 0 2.5 5.0 10
GSK715 (μM) GSK025 (μM)
G
OVCAR8
MDA-MB-231
C 1 2 C 1 2
sgPRMT1 sgPRMT5
H
ERCC1 Luc activity
DMSO
G715
G025
Basic ERCC1
Control
PRMT1-sg1
PRMT1-sg2
PRMT5-sg1
PRMT5-sg2
Basic ERCC1
I
UV exposure
CPD
Anti-CPD ab
ERCC1-XPF
Dimer excision
1. PRMTi pre-treatment
48 hrs
2. UV exposure
4 hrs
3. IF or DNA blots
J
No UV
DMSO
G715
G025
CPD
DAPI
Relative intensity
K
Control
PRMT1 sg1
PRMT1 sg2
PRMT5 sg1
PRMT5 sg2
L
NC D G715 D G025
100 ng
50 ng
25 ng
M
sgPRMT1 sgPRMT5
C 1 2 C 1 2
N
OVCAR8
MDA-MB-231
ERCC1
Tubulin
C 1 2
sgERCC1
O
Control
ERCC1 sg1
ERCC1 sg2
Olap DMSO 0 0.5 1 1.5 2 2.5 3 3.5 4
(nM log10)
Survival fraction
ERCC1sg1
ERCC1sg2
P
Control
ERCC1
Olap
G715
G025
Com
Control-GSK715
Control-Olaparib
Control-Combination
ERCC1-GSK715
ERCC1-Olaparib
ERCC1-Combination
Control-GSK025
ERCC1-GSK025

Figure 5.

ERCC1 repression is a common mechanism by which PRMTis sensitize cells to PARPi treatment

A. A siRNA screen was performed to evaluate the effects of knocking down the candidate genes on PARPi sensitivity in MDA-MB-231 cells. Gray: control siRNA transfection. **B.** Schematic of the impact score estimation for each candidate gene based on RNA-seq and a siRNA screen. **C.** Summary of the impact scores of 13 examined candidates. **D.** Expressional differences in ERCC1 mRNA levels between tumor specimens and their corresponding controls. Red and blue indicate up and down-regulation, respectively. Size: fold change, intensity: p-value. **E.** Correlations of mRNA expression levels between ERCC1 and PRMT1 (left) and PRMT5 (right) across all the TCGA tumors. Color indicates cancer type. **F.** Western blot analysis of ERCC1 protein expression in cancer cells treated with different GSK3368715 and GSK3235025 concentrations, independently, for 72 h. **G.** Western blot analysis of ERCC1 protein expression in OVCAR8 and MDA-MB-231 cells in which PRMT1 and PRMT5 were independently knocked out using lentiviral CRISPR/Cas9. **H.** Luciferase reporter assay of ERCC1 core promoter activity in HEK293T cells treated with GSK3368715 (5 μM, 48 h) and GSK3235025 (5 μM, 48 h) independently (upper panel), or after knocking out PRMT1 and PRMT5, independently (lower panel). Statistical difference was assessed using Student's t test, *p < 0.05; n =3. Error bars represent means ± SDs. **I.** Schematic of UV-induced cyclobutane pyrimidine dimers (CPD) detection by antibody (upper panel) and the experimental schedule (lower panel). **J.** Representative images (left) and quantitative results (right) of UV-induced CPD formation in MDA-MB-231 cells treated independently with DMSO, GSK3368715 (2.5 μM, 96 h), and GSK3235025 (5 μM, 96 h). Cells not subjected to UV treatment were used as the negative control. Scale bars, 10 μm. Statistical analysis by Student's t test, *p < 0.05; n = 3. Error bars represent means ± SD. **K.** Representative images (left) and quantitative results (right) of UV-induced CPD formation in MDA-MB-231 cells in which PRMT1 and PRMT5 were independently knocked out using lentiviral CRISPR/Cas9. Scale bars, 10 μm. Statistical differences were assessed using Student's t test, *p < 0.05; n = 3. Error bars represent means ± SDs. **L.** Dot blots of CPD levels in MDA-MB-231 cells treated independently with DMSO, GSK3368715 (5 μM, 96 h), and GSK3235025 (5 μM, 96 h). Cells not subjected to UV treatment were used as the negative control. Methylene blue staining was used as the loading control. **M.** Dot blots of CPD levels in MDA-MB-231 cells in which PRMT1 and PRMT5 were independently knocked out using lentiviral CRISPR/Cas9. Methylene blue staining was used as the loading control. **N.** Western blot analysis of ERCC1 protein expression in OVCAR8 and MDA-MB-231 cells in which PRMT1 and PRMT5 were independently knocked out using lentiviral CRISPR/Cas9. **O.** Sensitivity of OVCAR8 and MDA-MB-231 cells to olaparib. Left panel: crystal violet staining of a colony formation assay; right panel: survival fraction quantified from the upper panel. **P.** Sensitivity of OVCAR8 and MDA-MB-231 cells, which overexpressed ERCC1 owing to a lentiviral infection, to olaparib, GSK3368715, GSK3235025, and combinations. Upper panel: crystal violet staining of a colony formation assay; lower panel: the survival fraction quantified from the upper panel.

PRMT inhibition activates intrinsic innate immune pathways in cancer cells

We also analyzed the PRMTi treatment-induced genes using a gene set enrichment analysis and found that the most upregulated pathways were associated with immune responses (**Figure 6A**). Using the immune-related gene list from an immune gene annotation database (ImmPort), 516 reliably detectable genes (RPKM >1 by RNA-seq) in MDA-MB-231 cells were defined as the immune-related genes. Consistently, we found that 17.8% and 23.6% were upregulated by GSK3368715 and GSK3235025 treatments, respectively (**Figure 6B**). Compared with the upregulated non-immune-related genes, a significant number of the immune-related genes were induced by PRMT inhibition (GSK3368715, p = 7.6e-9; GSK3235025, p = 1.8e-18). Notably, 53 immune-related genes were upregulated by both PRMTis, and 37.7% of them were classified as innate immune-related genes by the InnateBD database (**Figure 6C**). These innate immune-related genes were associated the major innate immune signaling pathways, such as cytokines, chemokines, and their receptors (**Figure 6D**). These results suggest that PRMTi treatments may enhance intrinsic immune

reactions in tumor cells, providing a strong rationale for the application of PRMTis (or in combination with immune checkpoint inhibitors) in immuno-oncology. Notably, PARPi treatments trigger anticancer innate immune responses by increasing cytosolic DNA. Consequently, using the phosphorylation of TBK1 as a functional marker to monitor the activities of innate immune signals in tumor cells, we found that the PRMTi treatment alone induced comparable levels of p-TBK1 as the PARPi treatment, whereas the combination of PRMTi and PARPi increased p-TBK1 remarkably compared with single agent treatments (**Figure 6E**). This observation was confirmed by genetically knocking down PRMT1 and PRMT5 independently using CRISPR/Cas9 (**Figure 6F**). Because both PRMTi and PARPi treatments induced DNA damage in cancer cells, we also examined cytoplasmic micronuclei using PicoGreen staining, which specifically recognizes dsDNA (**Figure 6G**). Indeed, the numbers of cytoplasmic micronuclei significantly accumulated when cells were treated with PRMTis or PARPi alone, whereas the combination treatment synergistically enhanced this response (**Figure 6H**). The combination of PRMTis and PARPi may synergistically enhance anticancer immunity because cytoplasmic dsDNA triggers the cGAS-STING-TBK1 pathway[102].

Type I PRMT and PRMT5 inhibition act synergistically to enhance PARPi sensitivity

The inhibition of type I PRMT and PRMT5 represses shared, as well as distinct, BRCAness genes (**Figure 4A**); consequently, we hypothesized that the combination of type I PRMT and PRMT5 inhibitors may act synergistically to enhance PARPi sensitivity. Thus, using ERCC1 as an example, we examined whether there was a synergistic effect on the repression of shared targets. Both chemical (PRMTis) and genetic (CRISPR) approaches demonstrated that the repression of both PRMT1 and PRMT5 more significantly reduced ECRR1 promoter activities than single treatments (**Figure 7A, B**). This transcriptional synergistic action was further confirmed by qRT-PCR (**Figure 7C**). More importantly, the combination treatment almost completely repressed ERCC1 protein expression in cancer cell lines (**Figure 7D**). Using combinations of inhibitors that target the same pathway or biological process not only leads to synergistic effects and overcomes resistance, it may also reduce the required dose of each drug, thereby reducing potential side effects and increasing the therapeutic window. For example, co-targeting type I PRMTs and PRMT5 using a combination of different PRMTis showed synergistic actions and promising therapeutic efficacies in preclinical models[48, 73, 74]. Because PARPis are well tolerated in clinical practice, we next evaluated whether de-escalation doses of PRMTis in combination with PARPi can achieve a therapeutic efficacy in a panel of cancer cells (**Figure 7E**). Decreased independent doses of GSK3368715 (125 nM) and GSK3235025 (500 nM) achieved identical synergistic effects as the original doses of these two inhibitors (**Figure 7E**). Furthermore, although extremely low doses of GSK3368715 (25 nM) and GSK3235025 (100 nM) independently showed moderate synergy with olaparib, and a triple combination produced a strong synergistic action with olaparib. More importantly, when we further reduced doses of PRMTis, synergistic effects were still achieved (i.e., GSK3368715 at 12.5 nM and GSK3235025 at 12.5 nM) in the triple combination setting (**Figure 7F**). Similar results were observed for another FDA-approved PARPi, rucaparib (**Figure 7G** and Figure S6). Finally, we validated our *in vitro* observations in preclinical models in *in vivo* experiments using low doses of PRMTis (**Figure 7H–K**). Consistently, olaparib in combination with GSK3368715 and GSK3235025 independently significantly reduced tumor growth *in vivo* compared with the olaparib treatment alone, although in this low-dose PRMTi setting, PRMTi alone showed no (GSK3235025) or modest (GSK3368715) effects on tumor growth. In addition, the triple combination achieved a stronger therapeutic effect compared with the double combinations. Notably, consistent with previous report[73], combinations of GSK3368715 and GSK3235025 also showed promising therapeutic effects compared with GSK3368715 and GSK3235025 alone. Importantly, no significant side effects were observed in PRMTi and PARPi combinations and the triple combination in this low-dose PRMTi setting (**Figure 7L**), suggesting that both double and triple combinations may be tolerable in future clinical developments.

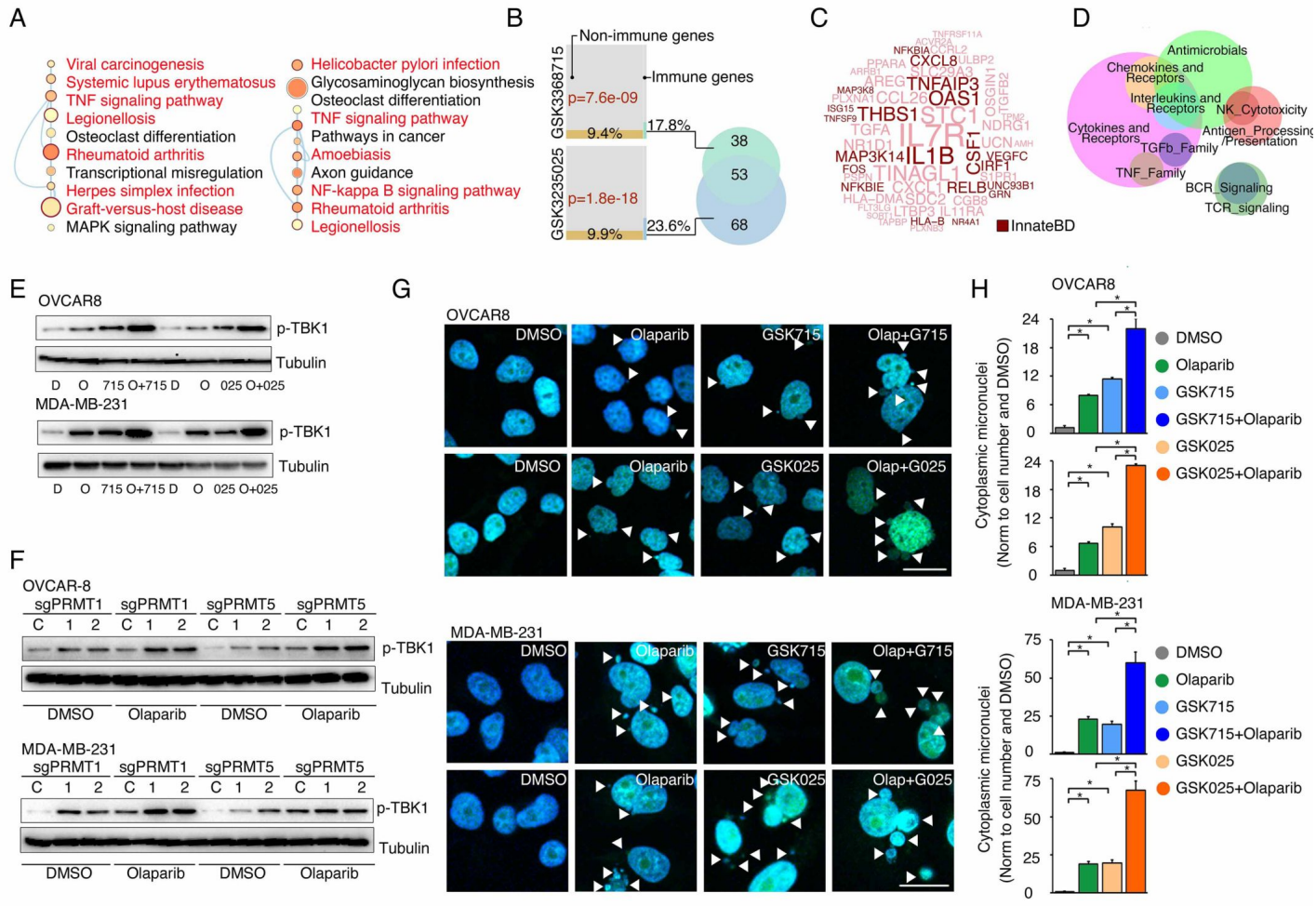

Figure 6.

PRMT inhibition activates intrinsic innate immune pathways in cancer cells

A. The top 10 KEGG pathways in which genes upregulated by GSK3368715 (left) and GSK3235025 (right) treatments were significantly enriched. Circle size indicates fold enrichment. Lines indicate numbers of shared genes between pathways. The immune-related pathways are highlighted in red. **B.** Mosaic plots show percentages of genes upregulated by GSK3368715 (upper) and GSK3235025 (lower) treatments. Right: immune-related genes, left: non-immune-related genes. Significantly more immune-related genes, compared with non-immune related genes, were upregulated by PRMT inhibition (GSK3368715:17.8% vs 9.4%; GSK3235025: 23.6% vs 9.9%). **C.** Word cloud revealing the common immune-related genes upregulated by GSK3368715 and GSK3235025 treatments. 37.7% are associated with innate immune responses (dark red). Text size indicates meta-fold changes by both PRMTis. **D.** Scaled Venn diagram showing the functional families among the common upregulated immune-related genes. **E.** Western blot analysis of p-TBK1 expression in OVCAR8 (upper panel) and MDA-MB-231 (lower panel) cells treated with DMSO, olaparib (5 μM), GSK3368715 (OVCAR8, 5 μM and MDA-MB-231, 2.5 μM), GSK3235025 (5 μM) or olaparib (5 μM) combined independently with GSK3368715 (OVCAR8, 5 μM and MDA-MB-231, 2.5μM) and GSK3235025 (5 μM) for 96 h. **F.** Western blot analysis of p-TBK1 expression in OVCAR8 (upper panel) and MDA-MB-231 (lower panel) cells in which PRMT1 and PRMT5 were independently knocked out using lentiviral CRISPR/Cas9. The cells were treated with olaparib (5 μM, 96 h) or DMSO. **G.** Representative cytoplasmic micronuclei stained by PicoGreen in OVCAR8 (upper panel) and MDA-MB-231 (lower panel) cells treated with DMSO, olaparib (5 μM), GSK3368715 (OVCAR8, 5 μM and MDA-MB-231, 2.5 μM), GSK3235025 (5 μM), and olaparib (5μM) combined independently with GSK3368715 (OVCAR8, 5 μM and MDA-MB-231, 2.5 μM) and GSK3235025 (5 μM). White arrows: micronuclei. Scale bar: 10 μm. **H.** Quantification of micronuclei from G. Micronuclei number per cell was normalized to DMSO. Statistical significance was assessed using a two-tailed Student's t test. Error bars represent means ± SDs.

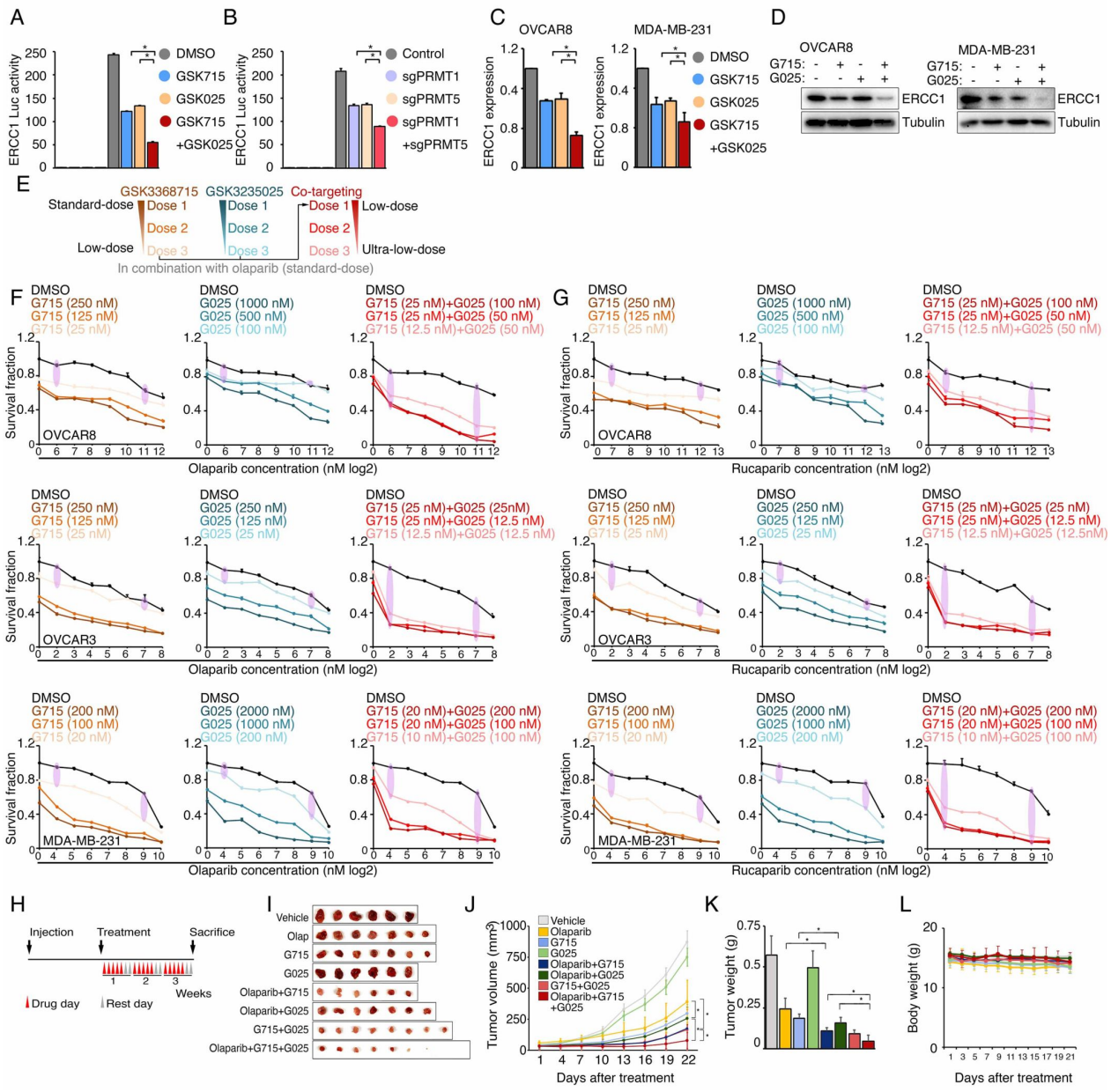
A
B
C
D
ERCC1 Luc activity
DMSO
GSK715
GSK025
GSK715 +GSK025
Control
sgPRMT1
sgPRMT5
sgPRMT1 +sgPRMT5
OVCAR8
MDA-MB-231
ERCC1 expression
G715:
G025:
ERCC1
Tubulin
E
GSK3368715
GSK3235025
Co-targeting
Standard-dose
Low-dose
Ultra-low-dose
Dose 1
Dose 2
Dose 3
In combination with olaparib (standard-dose)
F
G
Survival fraction
OVCAR8
OVCAR3
MDA-MB-231
Olaparib concentration (nM log2)
Rucaparib concentration (nM log2)
H
Injection
Treatment
Sacrifice
Drug day
Rest day
Weeks
I
Vehicle
Olap
G715
G025
Olaparib+G715
Olaparib+G025
G715+G025
Olaparib+G715+G025
J
Tumor volume (mm³)
Days after treatment
K
Tumor weight (g)
L
Body weight (g)
Days after treatment

Figure 7.

Type I PRMT and PRMT5 inhibition acts synergistically to enhance PARPi sensitivity

A. Luciferase reporter assay of the ERCC1 core promoter activity levels in HEK293T cells treated with DMSO, GSK3368715 (5 μM, 48 h), and GSK3235025 (5 μM, 48 h) independently, or with the combination of GSK3368715 (5 μM, 48 h) and GSK3235025 (5 μM, 48 h). Statistical differences were assessed using Student's t test, *p < 0.05; n = 3. Error bars represent means ± SDs. **B.** Luciferase reporter assay of the ERCC1 core promoter activity levels in HEK293T cells in which PRMT1, PRMT5, and PRMT1/5 were independently knocked out using lentiviral CRISPR/Cas9. Statistical differences were assessed using Student's t test, *p < 0.05; n = 3. Error bars represent means ± SDs. **C.** qRT-PCR analysis of ERCC1 RNA expression in OVCAR8 and MDA-MB-231 cells treated with GSK3368715 (5 μM) and GSK3235025 (5 μM) independently for 48 h. **D.** Western blot analysis of ERCC1 protein expression in OVCAR8 and MDA-MB-231 cells treated with GSK3368715 (5 μM) and GSK3235025 (5 μM) independently for 72 h. **E.** Dose de-escalation scheme. The lowest doses of GSK3368715 and GSK3235025 independently for PRMTi and the PARPi combination were first identified. They were then used as initial doses for triple combination. The doses of GSK3368715 and GSK3235025 were further reduced until the lowest doses for each PRMTi in the triple combination was identified. **F.** Sensitivity levels of OVCAR8 (upper panel), OVCAR3 (middle panel), and MDA-MB-231 (lower panel) cells to olaparib alone or olaparib combined with three different doses of GSK3368715 (left panel), GSK3235025 (middle panel), and GSK3368715 plus GSK3235025 (right panel). **G.** Sensitivity levels of OVCAR8 (upper panel), OVCAR3 (middle panel), and MDA-MB-231 (lower panel) cells to rucaparib alone or rucaparib combined with three different doses of GSK3368715 (left panel), GSK3235025 (middle panel), and GSK3368715 plus GSK3235025 (right panel). **H.** Schematic of the MDA-MB-231 xenograft experimental design. MDA-MB-231 cells were implanted subcutaneously in mice and grown until tumors reached a size of approximately 30 mm^3. Tumor-bearing mice were randomized and then received vehicle, 50 mg/kg olaparib i.p., 25 mg/kg GSK3368715 p.o., 50 mg/kg GSK3235025 p.o., or combinations of two agents or three agents, 5 days a week for 3 weeks. Caliper measurements were taken every other day from the initiation of drug treatment. **I.** Images of tumors collected from animals receiving vehicle, olaparib, GSK3368715, GSK3235025, and combinations of two agents or three agents. **J.** Tumor growth curve for each treatment group. Statistical significance was assessed using a two-tailed Student's t test. Error bars represent means ± SDs. **K.** Bar plot showing the mean tumor volume of each treatment group. Statistical significance was assessed using a two-tailed Student's t test. Error bars represent means ± SDs. **L.** Changes in the body weights of different murine treatment groups. Statistical significance was assessed using a two-tailed Student's t test. Error bars represent means ± SDs.

Discussion

An "induced PARPi sensitivity by epigenetic modulation" strategy (i.e., epigenetically impairing the genes of the DDR pathway in HR-proficient tumors to induce an HR-deficiency or other DDR-defects, thereby enhancing and sensitizing tumor cells to PARPi) has been developed recently to expand PARPi clinical applications[9, 10, 15]. For example, our previous study has demonstrated that repression of BET activity can significantly reduce the expression levels of essential HR genes by inhibiting the transcriptional activities of their super enhancers[15]. This preclinical discovery is being evaluated in a Phase 1b/2 clinical trial (NCT03901469) by a combination of BETi (ZEN-3694) with PARPi (talazoparib) for treatment of patients with metastatic TNBC without germline BRCA1/2 mutations (i.e., intrinsic HR-proficient patients)[34]. Excitingly, promising anti-cancer activity of this novel drug combination has been observed in the on-going clinical trial. Importantly, paired tumor biopsies have shown robust target engagement (repression of BRCA1 and RAD51 mRNA expression)[34], consistent with our preclinical studies in xenograft tumor models[15]. This trial is being expanded to a Phase 2b stage to accrue additional patients with TNBC. In addition, other combination approaches[15–33] based on the "induced PARPi sensitivity by epigenetic modulation" strategy also achieved promising clinical responses in

intrinsic or acquired HR-proficient settings[23, 28–31, 34]. Most importantly, due to cancer cells being extremely sensitive to the epigenetic repression of DDR genes compared with normal cells, the clinical studies demonstrated that this strategy is well tolerable for the patients with cancer.

However, two key clinically challenges still need to be addressed for future expansion of the application of this strategy in oncology: i.e., which clinically applicable epi-drug(s) can provide the strongest synergistic effects with PARPi? and can a BRCA-independent strategy be developed? To design and evaluate highly effective and BRCA-independent epi-drug/PARPi combination strategy, we performed a drug screen by combining olaparib, an FDA-approved PARPi, with a set of clinical applicable epi-drugs, which contain 74 well-characterized epigenetic modulators that target five major classes of epigenetic enzymatic actions. Among them, 7 are FDA-approved drugs in oncology, and 14 and 54 are in clinical trials and preclinical development, respectively. Notably, both type I PRMTi and PRMT5i exhibited high combination and clinical priority scores in our screen. This result was further confirmed by using different FDA-approved PARPis in multiple HGSOC and TNBC cell lines. Our functional studies demonstrated that PRMT inhibition significantly enhanced PARPi treatment-induced DNA damage in HR-proficient cancer cell lines. In consistency with the significant and positive correlation between the expression of PRMTs and DDR genes across primary cancer specimens, we observed that PRMT activities maintain the transcription of genes associated with DNA damage repair and “BRCAness” in cancer cells.

The expression levels of many PRMT family members are significantly elevated in cancer cells and associated with poor clinical outcomes, strongly suggesting that they may serve as a class of novel therapeutic targets in oncology. Our large-scale genomic and functional profiles from TCGA and DepMap further confirm that PRMT1, PRMT4, and PRMT5 are potential therapeutic targets in oncology. Major pharmaceutical companies have developed more than ten selective and potent PRMTis that are currently undergoing early-stage clinical evaluation. Development of novel treatment strategy to expand its potential clinical application is a key challenge for application of PRMTis in oncology. Given that recent clinical trials indicate that the activity of PRMTi alone may be insufficient to manage patients with cancer[81–88], even in MTAP-deletion setting, therefore, the design and evaluation of combination approaches using PRMTi with other therapeutic drugs are urgently needed. Our preclinical studies provide a strong rationale for a combination of PRMTi with PARPi for treatment of patients with HR-proficient HGSOC or TNBC. In addition, this strategy may also be expanded to other cancer types such as prostate and pancreatic cancers, in which PARPi has been approved by the FDA for clinical management.

As major histone modifiers, PRMTs control methylation of histones, thereby epigenetically regulating gene transcription and expression[35–39]. Additionally, through protein post-translational modification, PRMTs also directly regulate non-histone protein functions. For examples, PRMTs preferentially modify the splicing factors to maintain appropriate splicing process in cells. Given that the PRMT-regulome broadly influences multiple cellular processes in cancer cells, the mechanisms of action for the PRMT and PARP inhibitor combination may be highly complicated and context-dependent. For example, it has been reported that PRMTs indirectly regulate DDR gene expression through their functions on maintaining arginine methylation of the proteins in splicing complex[59, 62, 66]. Consistent with these studies, we also found that splicing of certain DDR genes, such as ERCC1, was impaired by PRMT inhibition. Additionally, PRMTs may also directly impact arginine methylation in certain DDR genes, thereby influencing their function in DNA damage response[52–58, 60, 61, 63, 65]. In the context of HGSOC/TNBC, our results suggest that treatment with both type 1 PRMT and PRMT5 inhibitors suppressed RNA expression of many genes potentially involved in PARP inhibitor sensitivity (i.e. BRCAness genes). Although some of them were inhibited by both inhibitors, type 1 PRMT and PRMT5 inhibitors repressed distinct BRCAness genes. Splicing alterations in certain BRCAness genes were identified after a PRMTi treatment, therefore, the PRMTi-treatment-induced splicing susceptibility may also serve as an alternative mechanism for the synergistic action of PRMTi and

PARPi. However, BRCAness genes were not significantly enriched among the genes whose splicing was significantly altered by PRMTi treatment, suggesting that splicing alteration might not serve as a dominant mechanism for PRMTi/PARPi combination, at least in the HGSOC/TNBC setting. Our studies not only provided mechanistic explanations for PRMTi and PARPi combinations but also provided novel information for the clinical development of this strategy. For example, ERCC1 expression may serve as a predictive biomarker for patient selection. Notably, ERCC1 is being evaluated in the clinic as a novel biomarker for predicting platinum sensitivity in lung cancer[98], [103]–[105]. Finally, tumor intrinsic genomic status may affect responses to PRMTi alone or combination treatments[35]–[39]. Supporting previous reports found that the Myc-PRMT loop plays critical roles during tumorigenesis[45], and "Myc-targets" signatures were the most significant signatures correlated with the expression of PRMT1 and PRMT5. Therefore, under MYC-hyperactivated condition, tumors may be extremely sensitive to PRMTis or PRMTi/PARPi combination.

Co-targeting type I PRMT and PRMT5 has shown strong synergistic actions and promising therapeutic efficacies[48], [73], [74]. Combinations of drugs that target the same pathway (e.g., combination of dabrafenib and tremetinib) not only lead to synergistic effects and overcome resistance, they may also reduce the required dose of each drug, decreasing side effects and increasing the therapeutic window[99]. In a PARPi treatment setting, type I PRMT and PRMT5 regulated shared as well as distinct BRCAness genes, suggesting that co-targeting type I PRMT and PRMT5 may produce a synergistic effect. Indeed, we observed that dual treatments of type I PRMT and PRMT5 more significantly reduced ECRR1 expression compared with single treatments. Notably, in consistence with previous reports[73], [99], PRMT5i increased global sDMA levels, which suggested that type I PRMT and PRMT5 share a substrate (i.e., MMA) and/or their functions are compensatory. Therefore, we believe that co-targeting type I PRMT and PRMT5 not only results in a synergistic effect that enhances PARPi sensitivity, reducing the required dose of each drug, but it also serves as a strategy to overcome potential resistance due to the compensatory functions of type I PRMT and PRMT5. This concept was supported by our *in vitro* triple combination experiments as well as *in vivo* studies. Although treatment-related adverse events are manageable and reversible with treatment interruption and reduction, efficacy of PRMTis as monotherapeutic agents was modest in clinical trials[81]–[88]. Therefore, novel combination strategies using lower doses of PRMTis urgently need to be designed and evaluated. Our studies indicated that, because PRMT "addiction" enables tumor cells to survive DNA damage, targeting PRMTs can lead to "treatment-induced DNA damage sensitivity", thereby sensitizing tumor cells to PARPi (and other DNA damaging drugs) treatments. A low-dose PRMTi in combination with PARPi may represent a more tolerable strategy for future clinical applications in oncology. Finally, co-targeting type I PRMT and PRMT5 may further significantly reduce the doses of each PRMTi (i.e., ultra-low-dose), thereby decreasing side toxicity effects of PRMTis. Taken together, our studies provide a strong rationale for clinical application of a combination of PRMT and PARP inhibitors in the patients with HR-proficient ovarian or breast cancer. Our mechanistical characterization may contribute to the future clinical development of PRMTis by defining mechanism of action, identifying rationales for combination, selecting response predictive biomarkers, and guiding dose and treatment schedules.

Materials and Methods

Cell culture

OVCAR8, OVCAR3, MDA-MB-231 and MDA-MB-468 cells were purchased from the ATCC or the NCI Development Therapeutics Program without further authentication. All cell lines were maintained at 37°C and 5% CO2. Cells were cultured in RPMI1640 medium (Invitrogen) supplemented with 10% fetal bovine serum (FBS, Invitrogen). Cells were routinely tested for mycoplasma contamination using Mycoplasma Plus PCR Primer Set (Agilent, Santa Clara, CA).

Drug combination screening and validation

OVCAR8 and MDA-MB-231 cells were used for drug combination screening. Before screening, each epigenetic inhibitor (n=74) was arrayed in 48-well plates at concentrations of 0.1 μM, 1 μM, 10 μM for IC50 calculation. For screening, cells were seeded in 48-well plates at a concentration of 3,750 cells/mL for OVCAR8 and 625 cells/mL for MDA-MB-231 in 400 μL of medium per well, and then treated with a single drug or with a combination of olaparib and one of the 74 epigenetic drugs 10 days for OVCAR8 or 8 days for MDA-MB-231. When testing for synergy of olaparib with epigenetic drugs, the drug combinations were plated with 5-point serially constant two-fold ratio dilutions in 48-well plates using Eppendorf Xplorer plus Electronic Single Channel Pipette. Drugs were changed every two days. Cell viability testing was performed using the crystal violet staining assay (Sigma). After crystal violet was dissolved in 2% SDS, absorbance value was measured at 590nm with spectrophotometer. Combination index (CI) and fraction affected (Fa) values were calculated using Compusyn software[106]. The synergistic action between PRMTis and PARPis were further validated in a panel of cancer cell lines. In addition, triple drug combination was also evaluated in the same cell lines. Detailed combination condition was listed in Table S9.

Colony formation assay

Cells were seeded in 48-well plates at a concentration of 3,750 cells/mL for OVCAR8, 10,000 cells/mL for OVCAR3, 625 cells/mL for MDA-MB-231 and 10,000 cells/mL for MDA-MB-468 in 400 μL of medium per well overnight. Cells were then treated with a single drug or a drug combination. After fixation with methanol, colonies were stained with 0.5% crystal violet for 30 min. For quantification, crystal violet was dissolved in 2% SDS and read by microplate reader.

CRISPR/Cas9 knockout

LentiCRISPRv2 was purchased from Addgene (plasmid #98290). sgRNAs targeting PRMT1, PRMT5 and ERCC1 were ordered from IDT and cloned to LentiCRISPRv2. LentiCRISPRv2 and packaging vectors were transfected into 293T cells. The medium was changed 8 hr after transfection, and the medium containing lentivirus was collected 48 hr later. Cancer cells were infected with lentivirus in the presence of 8 μg/ml polybrene. 24 hours post-infection, infected cells were selected with 1 μg/mL puromycin and the surviving pools were expanded for the following experiments.

Protein isolation and Western blot

Western blotting was performed using the following primary antibodies: anti-PRMT1 (Cat No: 2449S, CST); anti-PRMT5 (Cat No: 79998S, CST); anti-aDMA (Cat No: 13522S, CST); anti-sDMA (Cat No: 13222S, CST); anti-ERCC1 (Cat No: 3885S, CST); anti-phospho-H2AX (S139) (Cat No: 05-636, Clone No: JBW301, Millipore); p-TBK1 (Cat No: 5483S, CST) and anti-β-Tubulin (Cat No: 2128, Clone No: 9F3, CST), followed by incubation with secondary antibodies conjugated with horseradish peroxidase (HRP, GE Healthcare Life Sciences). Immunoreactive proteins were visualized using the LumiGLO chemiluminescent substrate (Cell Signaling).

Comet assays

For PRMT1/5 inhibitors treatment comet assay, OVCAR8 cells were treated with DMSO, 5 μM olaparib, 5 μM GSK3368715, 5 μM olaparib combined with 5 μM GSK3368715, 5 μM GSK3235025 and 5 μM olaparib combined with 5 μM GSK3368715 for 96 hours. OVCAR3 cells were treated with DMSO, 1 μM olaparib, 1 μM GSK3368715, 1 μM olaparib combined with 1 μM GSK3368715, 1 μM GSK3235025 and 1 μM olaparib combined with 1 μM GSK3368715 for 96 hours. MDA-MB-231 cells were treated with DMSO, 5 μM olaparib, 2.5 μM GSK3368715, 5 μM olaparib combined with 2.5 μM GSK3368715, 5 μM GSK3235025 and 5 μM olaparib combined with 5 μM GSK3368715 for 96 hours. MDA-MB-468 cells were treated with DMSO, 2.5 μM olaparib, 2.5 μM GSK3368715, 2.5 μM olaparib combined with 2.5 μM GSK3368715, 5 μM GSK3235025 and 2.5 μM olaparib combined with 5 μM

GSK3368715 for 96 hours. For PRMT1/5 KO comet assay, wide type, PRMT1 sgRNA KO and PRMT5 sgRNA KO cells were treated with 5 μM olaparib for 96 hours. Neutral comet assays with SYBR gold staining (Invitrogen) were performed. The quantification of tail DNA was done using CASP software.

Immunofluorescent staining

For CPD foci staining, DMSO, 2.5 μM GSK3368715 (MDA-MB-231) or 5 μM GSK3368715 (OVCAR8), 5 μM GSK3235025 treated cells or PRMT1/5 KO cells were irradiated with UV (15 J/m^2) and then allowed to repair for indicated times in fresh medium. Cells were fixed in solution containing 3% paraformaldehyde and 2% sucrose for 10 min at room temperature. Cells were subsequently permeabilized with 0.5% Triton solution for 5 min at 4°C and then incubated with anti-CPD antibody (Cat No: CAC-NM-DND-001, Cosmo Bio LTD) in PBST buffer (PBS plus 0.1% Tween-20, 0.02% NaN3) overnight at 4°C. Cells were then washed three times with PBST and then incubated with goat anti-mouse IgG cross-adsorbed secondary antibody, Alexa Fluor 488 (Cat No: A-11017, Thermo) for 1 hour at room temperature. After four washes with PBST, coverslips were mounted onto glass slides using Vectashield mounting medium containing DAPI (Vector Laboratories) and visualized using an Axiovert 200M inverted microscope (Zeiss). For PicoGreen micronuclei staining, DMSO, 2.5 μM GSK3368715 (MDA-MB-231) or 5 μM GSK3368715 (OVCAR8), 5 μM GSK3235025 treated cells were fixed in solution containing 3% paraformaldehyde and 2% sucrose for 10 min at room temperature. Cells were subsequently permeabilized with 0.5% Triton solution for 5 min at 4°C and then incubated with PicoGreen (1:1000 dilution) (Cat No: P11496, ThermoFisher Scientific) in PBST buffer (PBS plus 0.1% Tween-20, 0.02% NaN3) overnight at 4°C. After four washes with PBST, coverslips were mounted onto glass slides using Vectashield mounting medium containing DAPI (Vector Laboratories) and visualized using an Axiovert 200M inverted microscope (Zeiss).

RNA isolation and qRT-PCR

Total RNA was extracted using TRIzol Reagent (Invitrogen) and reverse transcribed using the High Capacity RNA-to-cDNA Kit (Applied Biosystems). cDNA was quantified by an ABI ViiA 7 System (Applied Biosystems). QPCR primers were listed in Table S10.

RNA-sequencing

MDA-MB-231 cells were treated with DMSO, olaparib (5μM, 6 days), GSK3368715 (2.5μM, 6 days), GSK3235025 (5μM, 6 days) or combinations. Following total RNA extraction, libraries were prepared using TruSeq Stranded mRNA Library Prep Kit (Illumina), and equimolar libraries were multiplexed and sequenced on an Illumina NextSeq 500 (pair end 100 bp reads) by the BGI Genomics. FASTQ files were downloaded for the analysis.

Splicing analysis

Paired end RNA-seq profiles were used to characterize treatment-induced splicing changes. Differential splicing was detected by rMATS algorithm (*http://rnaseq-mats.sourceforge.net/download.html*), using a hierarchical framework to model exon inclusion levels[107, 108]. Five alternative splicing events were identified, including skipped exon (SE), alternative 5' splice site (A5SS), alternative 3' splice site (A3SS), mutually exclusive exons (MXE), and retained intron (RI).

ERCC1 overexpression

For ERCC1 overexpression, OVCAR8 and MDA-MB-231 cells were seeded in 12-well plates at a confluence of 50% one day before transduction. Cells were transduced with lentiviral CD513B vector (System Biosciences) or CD513B-ERCC1. Medium was changed the next day. Cells were

selected with 5 μg/ml puromycin for 3 days, then seeded for sensitivity detection of olaparib alone, GSK3368715 alone /GSK3235025 alone, or combination of olaparib with GSK3368715 or GSK3235025.

DNA dot-blot

Cells were irradiated with UV (15 J/m^2) and then allowed to repair for indicated times in fresh medium. Genomic DNA was extracted from these UV-irradiated cells using the QIAamp DNA Blood Mini Kit (51104, Qiagen) and RNase A (19101, Qiagen). DNA solutions were prepared in 50 μL of PBS per sample to have 100 ng, 50 ng and 25 ng of genomic DNA. DNA solutions were spotted onto Hybond-N+ positively charged nylon membrane (RPN1210B, GE Healthcare). Membranes were blocked at room temperature for 1 hour in TBS-T (Tris-Buffered Saline (TBS), 0.05% Tween-20) containing 5% skim milk, and incubated with the anti-CPD antibody. Membranes were washed four times in TBS–T, then incubated for 1 hour with the appropriate peroxidase-conjugated anti-mouse secondary antibody at 1/5,000 (EMD Millipore). Immunoreactive proteins were visualized using the LumiGLO chemiluminescent substrate (Cell Signaling).

Luciferase assays

-1500 ~ +120 bp of ERCC1 promoter was cloned into the pGL3-basic reporter vector (Promega) to make a ERCC1-P-Luc luciferase reporter plasmid. For drug treatment reporter assay, 500 ng of reporter vector plus 50 ng of the renilla luciferase plasmid was transfected to cells using FuGENE 6 (Promega); cells were then treated with DMSO, 5 μM GSK3368715 and 5 μM GSK3235025 for 48 hours. For PRMT1 and PRMT5 CRISPR KO reporter assay, cells infected with control, PRMT1-sgRNA and PRMT5-sgRNA lentivirus were then transfected with reporter vector and renilla, and cells were harvested 48 hours after transfection. Reporter assays were performed using a dual luciferase reporter assay system (Promega) by Fluoroskan Ascent FL fluorometer (Thermo Fisher Scientific).

In vivo treatment experiment

For MDA-MB-231 xenograft experiments, three million tumor cells were injected subcutaneously into 6-weeks-old athymic female nu/nu mice (Stock No: 002019, Jackson Labs) and grown until tumors reached a size of approximately 30 mm^3. Xenografted mice were randomized and then received vehicle, 50 mg/kg olaparib ip, 25 mg/kg GSK3368715 po, 50 mg/kg GSK3235025 po or the combination of two agents and three agents, 5 days a week for 3 weeks (n=6~8 per group). Caliper measurements were taken every three days starting from the initiation of drug treatment. Tumor volumes were calculated according to the formula: tumor volume [mm^3] = (1/6) × π × (tumor length) × (tumor width)^2. Due to the nature of the performed experiments, no randomization and no blinding was used because it was deemed unfeasible. However, the resulting tumors were analyzed in a blinded manner. All animal procedures were in accordance with protocols approved by the Institutional Animal Care and Use Committee of the University of Pennsylvania.

Estimation of impact score of siRNA experiment

For a specific gene g, we used $\exp(t)_g$ to represent its expression measured by RNA-seq in a cell line treated with a given drug t, and $\exp C_g$ to represent its expression in a control treatment. Fold changes of expression were calculated for a specific gene by comparing its expression in each treatment condition to control treatment,

$$Fexp(t)_g = \log_2\left(\exp(t)_g\right) - \log_2\left(\exp C_g\right).$$

For a specific gene g, we used $IC50(k)_g$ to represent IC50 of PARPi treatment in a cell line after knockdown this gene by pooled siRNA transfection, and IC50C to represent IC50 of PARPi treatment in a control siRNA transfection. Fold changes of IC50 were calculated for a specific gene

knockdown by comparing PARPi IC50 in the same cell line in siRNA knockdown condition to control siRNA transfection,

$$FIC50(k)_g = \frac{\text{IC50}(k)_g}{\text{IC50C}}.$$

Fold changes of IC50 were then normalized by min-max feature scaling,

$$F'IC50(k)_g = \frac{FIC50(k)_g - FIC50(k)_{min}}{FIC50(k)_{max} - FIC50(k)_{min}}.$$

A final priority score was calculated for each gene examined,

$$Score_g = F'IC50(k)_g * \sum Fexp(t)_g.$$

TCGA RNA-seq data processing and gene expression analysis

The poly(A)+ RNA-seq data for primary tumors and their adjacent tissues were generated by the University of North Carolina and the British Columbia Cancer Agency Genome Sciences Centre as part of the TCGA project. All RNA-seq data were processed through a pipeline developed by the UCSC Toil RNAseq Recompute Compendium, which allowed us to consistently process large-scale RNA-seq data without computational batch effects [109]. For TCGA RNA-seq data, if more than one sample existed for a participant, one single tumor sample (and matched adjacent sample, if applicable) was selected based on the following rules: (1) tumor sample type: primary (01) > recurrent (02) > metastatic (06); (2) order of sample portions: higher portion numbers were selected; and (3) order of plate: higher plate numbers were selected.

TCGA mRNA differential expression meta-analysis

For each cancer type which had at least three normal tumor-adjacent tissues in TCGA, differential gene expression analysis between tumor tissues and normal tumor-adjacent tissues was performed using one sided *t*-test (for up-regulation and down-regulation respectively). P values across all cancer types were then combined via Fisher's combined probability test[110] to yield a meta-p value to assess the degree of up-regulation or down-regulation at the pan-cancer level. The meta-p value on the direction with the more significant dysregulation was reported for the corresponding PRMT genes.

CPTAC proteomic data processing and protein expression analysis

Extensive mass spectrometry-based proteomics data using isobaric tagging approaches (iTRAQ or TMT) for selected cancer types were generated by the National Cancer Institute's (NCI's) CPTAC. Protein-level processed data consisting of iTRAQ or TMT log(ratios) were downloaded from the CPTAC data portal (*https://cptac-data-portal.georgetown.edu*) on January 28, 2021.

CPTAC protein differential expression meta-analysis

Differential expression analysis between tumor tissues and paired normal tissues was performed using one sided *t*-test (for up-regulation and down-regulation respectively). P values across all cancer types were then combined via Fisher's combined probability test[110] to yield a meta-p value to assess the degree of up-regulation or down-regulation at the pan-cancer level. The meta-p value on the direction with the more significant dysregulation was reported for the corresponding PRMT.

TCGA survival meta-analysis

For each PRMT gene in a given cancer type, we fit a Cox proportional hazards model and obtained a z-statistic and a p-value (with direction of effect) to assess whether high expression was associated with favorable or unfavorable overall survival. P-values across all cancer types were

then combined via Fisher's combined probability test[110] to yield a meta-p value to assess the prognostic value at pan-cancer levels (for risky effect and protective effect separately). The meta-p value on the direction with the more significant prognostic association was reported for the corresponding PRMT gene.

Recurrent genomic analysis

Recurrent somatic copy number alterations and mutations of the PRMT family were analyzed in the TCGA sample cohort by a standard pipeline developed by the Functional Cancer Genome project[111–113]. The G-score (somatic copy number alterations) and M-score (mutations) were established for each PRMT gene at both individual and pan-cancer levels.

Statistical analysis

Large-scale and multi-dimensional profiling data generated by the publicly accessible databases (TCGA, CPTAC, and DepMap) were used, therefore statistical analysis was not used to predetermine sample size in this study. For TCGA analysis, if more than one profiling file existed for a patient in TCGA, only one single file will be selected and used, and detailed methods for exclusion of duplicated profiling files are described in the method section. The computational analyses were not randomized, and the investigators were not blinded during data analyses of this study. When applicable, enrichment was tested using Fisher's exact test with FDR correction. Cell viability and gene relative expression data were shown as means with standard deviation (SD). Comparisons between groups were performed using student t-test.

Data and code availability

The genomic profiles of human cancers were generated by the TCGA project, which are publicly available through the Genomic Data Commons portal (GDC, *https://gdc-portal.nci.nih.gov*). Protein-level processed data consisting of iTRAQ or TMT log(ratios) were downloaded from the CPTAC data portal (*https://cptac-data-portal.georgetown.edu*). Genetic screening profiles in human cancer cell lines were generated by the DepMap and the Score projects, which are publicly available through the DepMap portal (*https://depmap.org/portal/*), and the Score projects (*https://score.depmap.sanger.ac.uk/*). The genomic data were retrieved, processed and analyzed through a master computational protocol developed by the Functional Cancer Genome project (FCG, *http://fcgportal.org/home/*) as described by our previous publications[111–113] as well as the method section. This paper does not report original code. Any additional information required to reanalyze the data reported in this work paper is available from the corresponding authors upon request.

Acknowledgements

L.Z. was supported by the Basser Center for BRCA and the US National Institutes of Health (NIH) grants (R01CA142776, R01CA190415, R01CA225929, R01CA262070, 1R01CA285598, and P50CA083638). Z.H. and L.Z. was supported by the Adenoid Cystic Carcinoma Research Foundation and Torrey Coast Foundation. X.H. was supported by the Ovarian Cancer Research Alliance. X.H. and Y.Z. were supported by the Foundation for Women's Cancer. Support of the core facilities was provided by a NIH Cancer Center Support Grant (P30CA016520) to Abramson Cancer Center.

Author contributions

Y.Z., M.X., X.H., and L.Z. conceived and designed the research. J.Y. and Z.H. performed the computational/bioinformatics analysis and statistical analysis. Y.Z., M.X., J.J, H.J. B.W. and J.S. performed the biological experiments. M.L., Y.F., K.T.M., J.L.T., O.T., and H.M.C. performed epigenetic inhibitor data collection and discussion on clinical oncology and drug development. Y.Z., M.X., X.H., and L.Z. wrote the paper.

Declaration of interests

L.Z. and X.H. report having received research funding from AstraZeneca, Bristol-Myers Squibb/Celgene, and Prelude Therapeutics. Y.Z. is employees of GlaxoSmithKline. O.T. and H.M.C. are employees of AstraZeneca.

List of supplemental tables

Table S1. List of the epigenetic modulators that were used in initial drug combination screen.

Table S2. List of the specimens that were used in this study from the TCGA project.

Table S3. Expression of the PRMTs across cancers.

Table S4. Recurrent genomic alterations of the PRMTs across cancers.

Table S5. Cell dependencies of PRMTs from the DepMap project.

Table S6. Correlations between the expression levels of PRMT1/5 and “50 hallmark” molecular signatures across the TCGA tumor specimens.

Table S7. List of the potential BRCAness genes in the human genome.

Table S8. List of the BRCAness genes that were repressed by PRMTi treatment.

Table S9. PRMTi and PARPi combination concentration in each cancer line.

Table S10. Primers and oligoes that were used in this study.

Figure S1. The sensitivity of cancer cells to PARPi alone, PRMTi alone, and a PARPi and PRMTi combination in a panel of HGSOC and TNBC cell lines. For each treatment, the upper panel shows crystal violet staining of a colony formation assay; the lower left panel shows a quantified survival fraction; and the lower right panel shows the CI values. Fa, fraction affected.

Figure S2. Expression levels of the PRMTs across the TCGA tumor specimens.

A. The heatmap of mRNA expression levels of PRMT family across the TCGA tumor samples. The intensity of heatmap color indicates the FPKM value for each percentile (25th, 50th, 75th, and 90th) of an individual PRMT gene in a given cancer type. **B.** The mRNA expression levels of the PRMT family in tumors compared with corresponding controls in the TCGA cohorts. Red and blue

indicate up and down-regulation, respectively. **C.** The protein expression levels of the PRMT family in tumors compared with corresponding controls in the CPTAC cohorts. Red and blue indicate up and down-regulation, respectively.

Figure S3. Comet assay was used to measure DNA damage in cancer cell lines in which PRMTs were inhibited by chemical compounds or genetic approach.

A. Left panels: A comet assay was used to measure DNA damage in OVCAR8, OVCAR3, MDA-MB-231, and MDA-MB-468 cell lines treated with DMSO, olaparib, GSK3368715, GSK3235025, or combinations. Scale bars, 10 μm. Right panels: The extent of DNA damage was quantified using the tail moment in comet assays of OVCAR8, OVCAR3, MDA-MB-231, and MDA-MB-468 cell lines treated with DMSO, olaparib, GSK3368715, GSK3235025, or combinations. Data are presented as means ± SDs, *$p < 0.05$ determined by two-tailed Student's t tests. **B.** Left panels: A comet assay was used to measure olaparib treatment-induced DNA damage in OVCAR8, MDA-MB-231, and MDA-MB-468 cell lines in which PRMT1 and PRMT5 were independently knocked out using lentiviral CRISPR/Cas9. Scale bars, 10 μm. Right panels: The extent of olaparib treatment-induced DNA damage was quantified using the tail moment in comet assays of OVCAR8, MDA-MB-231, and MDA-MB-468 cell lines in which PRMT1 and PRMT5 were independently knocked out using lentiviral CRISPR/Cas9. Data are presented as means ± SDs, *$p < 0.05$ determined by two-tailed Student's t tests.

Figure S4. The expression levels of aDMA and sDMA in cancer cell lines in which PRMTs were inhibited by chemical compounds or genetic approach.

A. The expression levels of aDMA and sDMA in cancer in OVCAR8, OVCAR3, MDA-MB-231, and MDA-MB-468 cell lines treated with GSK3368715 or GSK3235025. **B.** The expression levels of aDMA and sDMA in cancer in OVCAR8 and MDA-MB-231cell lines in which PRMT1 or PRMT5 was knocked out by CRISPR/Cas9.

Figure S5. Dot blots of CPD levels in MDA-MB-231 cells in which ERCC1 was knocked out using lentiviral CRISPR/Cas9. Methylene blue staining was used as the loading control.

Figure S6. PRMT1 and PRMT5 inhibition acts synergistically to enhance PARPi sensitivity in a panel of HGSOC and TNBC cell lines.

References

1. Cancer Genome Atlas Research, N. (2011) **Integrated genomic analyses of ovarian carcinoma** *Nature* **474**:609–615

2. Cancer Genome Atlas N. (2012) **Comprehensive molecular portraits of human breast tumours** *Nature* **490**:61–70

3. Bowtell D.D., et al. (2015) **Rethinking ovarian cancer II: reducing mortality from high-grade serous ovarian cancer** *Nat Rev Cancer* **15**:668–679

4. Bianchini G., De Angelis C., Licata L., Gianni L (2022) **Treatment landscape of triple-negative breast cancer - expanded options, evolving needs** *Nat Rev Clin Oncol* **19**:91–113

5. Scott C.L., Swisher E.M., Kaufmann S.H (2015) **Poly (ADP-ribose) polymerase inhibitors: recent advances and future development** *J Clin Oncol* **33**:1397–1406

6. Pommier Y., O'Connor M.J., de Bono J (2016) **Laying a trap to kill cancer cells: PARP inhibitors and their mechanisms of action** *Sci Transl Med* **8**

7. Lord C.J., Ashworth A (2017) **PARP inhibitors: Synthetic lethality in the clinic** *Science* **355**:1152–1158

8. Dias M.P., Moser S.C., Ganesan S., Jonkers J (2021) **Understanding and overcoming resistance to PARP inhibitors in cancer therapy** *Nat Rev Clin Oncol* **18**:773–791

9. Konstantinopoulos P.A., Ceccaldi R., Shapiro G.I., D'Andrea A.D (2015) **Homologous Recombination Deficiency: Exploiting the Fundamental Vulnerability of Ovarian Cancer** *Cancer Discov* **5**:1137–1154

10. Pilie P.G., Tang C., Mills G.B., Yap T.A (2019) **State-of-the-art strategies for targeting the DNA damage response in cancer** *Nat Rev Clin Oncol* **16**:81–104

11. Curtin N.J (2012) **DNA repair dysregulation from cancer driver to therapeutic target** *Nat Rev Cancer* **12**:801–817

12. O'Connor M.J (2015) **Targeting the DNA Damage Response in Cancer** *Mol Cell* **60**:547–560

13. Pearl L.H., Schierz A.C., Ward S.E., Al-Lazikani B., Pearl F.M (2015) **Therapeutic opportunities within the DNA damage response** *Nat Rev Cancer* **15**:166–180

14. Groelly F.J., Fawkes M., Dagg R.A., Blackford A.N., Tarsounas M (2022) **Targeting DNA damage response pathways in cancer** *Nat Rev Cancer*

15. Yang L., et al. (2017) **Repression of BET activity sensitizes homologous recombination-proficient cancers to PARP inhibition** *Sci Transl Med* **9**

16. Karakashev S., et al. (2017) **BET Bromodomain Inhibition Synergizes with PARP Inhibitor in Epithelial Ovarian Cancer** *Cell Rep* **21**:3398–3405

17. Sun C., et al. (2018) **BRD4 Inhibition Is Synthetic Lethal with PARP Inhibitors through the Induction of Homologous Recombination Deficiency** *Cancer Cell* **33**:401–416

18. Johnson S.F., et al. (2016) **CDK12 Inhibition Reverses De Novo and Acquired PARP Inhibitor Resistance in BRCA Wild-Type and Mutated Models of Triple-Negative Breast Cancer** *Cell Rep* **17**:2367–2381

19. Iniguez A.B., et al. (2018) **EWS/FLI Confers Tumor Cell Synthetic Lethality to CDK12 Inhibition in Ewing Sarcoma** *Cancer Cell* **33**:202–216

20. Shan W., et al. (2020) **Systematic Characterization of Recurrent Genomic Alterations in Cyclin-Dependent Kinases Reveals Potential Therapeutic Strategies for Cancer Treatment** *Cell Rep* **32**

21. Muvarak N.E., et al. (2016) **Enhancing the Cytotoxic Effects of PARP Inhibitors with DNA Demethylating Agents - A Potential Therapy for Cancer** *Cancer Cell* **30**:637–650

22. Abbotts R., et al. (2019) **DNA methyltransferase inhibitors induce a BRCAness phenotype that sensitizes NSCLC to PARP inhibitor and ionizing radiation** *Proc Natl Acad Sci U S A* **116**:22609–22618

23. Baer M.R., et al. (2022) **Phase I Clinical Trial of DNA Methyltransferase Inhibitor Decitabine and PARP Inhibitor Talazoparib Combination Therapy in Relapsed/Refractory Acute Myeloid Leukemia** *Clin Cancer Res* **28**:1313–1322

24. Adimoolam S., et al. (2007) **HDAC inhibitor PCI-24781 decreases RAD51 expression and inhibits homologous recombination** *Proc Natl Acad Sci U S A* **104**:19482–19487

25. Konstantinopoulos P.A., Wilson A.J., Saskowski J., Wass E., Khabele D (2014) **Suberoylanilide hydroxamic acid (SAHA) enhances olaparib activity by targeting homologous recombination DNA repair in ovarian cancer** *Gynecol Oncol* **133**:599–606

26. Ibrahim Y.H., et al. (2012) **PI3K inhibition impairs BRCA1/2 expression and sensitizes BRCA-proficient triple-negative breast cancer to PARP inhibition** *Cancer Discov* **2**:1036–1047

27. Juvekar A., et al. (2012) **Combining a PI3K inhibitor with a PARP inhibitor provides an effective therapy for BRCA1-related breast cancer** *Cancer Discov* **2**:1048–1063

28. Konstantinopoulos P.A., et al. (2019) **Olaparib and alpha-specific PI3K inhibitor alpelisib for patients with epithelial ovarian cancer: a dose-escalation and dose-expansion phase 1b trial** *Lancet Oncol* **20**:570–580

29. Batalini F., et al. (2022) **Phase 1b Clinical Trial with Alpelisib plus Olaparib for Patients with Advanced Triple-Negative Breast Cancer** *Clin Cancer Res* **28**:1493–1499

30. Yap T.A., et al. (2020) **Phase I Trial of the PARP Inhibitor Olaparib and AKT Inhibitor Capivasertib in Patients with BRCA1/2- and Non-BRCA1/2-Mutant Cancers** *Cancer Discov* **10**:1528–1543

31. Westin S.N., et al. (2021) **Phase Ib Dose Expansion and Translational Analyses of Olaparib in Combination with Capivasertib in Recurrent Endometrial, Triple-Negative Breast, and Ovarian Cancer** *Clin Cancer Res* **27**:6354–6365

32. Mo W., et al. (2016) **mTOR Inhibitors Suppress Homologous Recombination Repair and Synergize with PARP Inhibitors via Regulating SUV39H1 in BRCA-Proficient Triple-Negative Breast Cancer** *Clin Cancer Res* **22**:1699–1712

33. Sun C., et al. (2017) **Rational combination therapy with PARP and MEK inhibitors capitalizes on therapeutic liabilities in RAS mutant cancers** *Sci Transl Med* **9**

34. Aftimos P.G., et al. (2022) **A phase 1b/2 study of the BET inhibitor ZEN-3694 in combination with talazoparib for treatment of patients with TNBC without gBRCA1/2 mutations** *Journal of Clinical Oncology* **40**:1023–1023

35. Blanc R.S., Richard S (2017) **Arginine Methylation: The Coming of Age** *Mol Cell* **65**:8–24

36. Guccione E., Richard S (2019) **The regulation, functions and clinical relevance of arginine methylation** *Nat Rev Mol Cell Biol* **20**:642–657

37. Jarrold J., Davies C.C (2019) **PRMTs and Arginine Methylation: Cancer's Best-Kept Secret?** *Trends Mol Med* **25**:993–1009

38. Lorton B.M., Shechter D (2019) **Cellular consequences of arginine methylation** *Cell Mol Life Sci* **76**:2933–2956

39. Wu Q., Schapira M., Arrowsmith C.H., Barsyte-Lovejoy D (2021) **Protein arginine methylation: from enigmatic functions to therapeutic targeting** *Nat Rev Drug Discov* **20**:509–530

40. Migliori V., et al. (2012) **Symmetric dimethylation of H3R2 is a newly identified histone mark that supports euchromatin maintenance** *Nat Struct Mol Biol* **19**:136–144

41. Cheung N., et al. (2016) **Targeting Aberrant Epigenetic Networks Mediated by PRMT1 and KDM4C in Acute Myeloid Leukemia** *Cancer Cell* **29**:32–48

42. Chiang K., et al. (2017) **PRMT5 Is a Critical Regulator of Breast Cancer Stem Cell Function via Histone Methylation and FOXP1 Expression** *Cell Rep* **21**:3498–3513

43. Pastore F., et al. (2020) **PRMT5 Inhibition Modulates E2F1 Methylation and Gene-Regulatory Networks Leading to Therapeutic Efficacy in JAK2(V617F)-Mutant MPN** *Cancer Discov* **10**:1742–1757

44. Bezzi M., et al. (2013) **Regulation of constitutive and alternative splicing by PRMT5 reveals a role for Mdm4 pre-mRNA in sensing defects in the spliceosomal machinery** *Genes Dev* **27**:1903–1916

45. Koh C.M., et al. (2015) **MYC regulates the core pre-mRNA splicing machinery as an essential step in lymphomagenesis** *Nature* **523**:96–100

46. Braun C.J., et al. (2017) **Coordinated Splicing of Regulatory Detained Introns within Oncogenic Transcripts Creates an Exploitable Vulnerability in Malignant Glioma** *Cancer Cell* **32**:411–426

47. Gerhart S.V., et al. (2018) **Activation of the p53-MDM4 regulatory axis defines the anti-tumour response to PRMT5 inhibition through its role in regulating cellular splicing** *Scientific Reports* **8**

48. Fong J.Y., et al. (2019) **Therapeutic Targeting of RNA Splicing Catalysis through Inhibition of Protein Arginine Methylation** *Cancer Cell* **36**:194–209

49. Radzisheuskaya A., et al. (2019) **PRMT5 methylome profiling uncovers a direct link to splicing regulation in acute myeloid leukemia** *Nat Struct Mol Biol* **26**:999–1012

50. Sachamitr P., et al. (2021) **PRMT5 inhibition disrupts splicing and stemness in glioblastoma** *Nat Commun* **12**

51. Li W.J., et al. (2021) **Profiling PRMT methylome reveals roles of hnRNPA1 arginine methylation in RNA splicing and cell growth** *Nat Commun* **12**

52. Boisvert F.M., Dery U., Masson J.Y., Richard S (2005) **Arginine methylation of MRE11 by PRMT1 is required for DNA damage checkpoint control** *Genes Dev* **19**:671–676

53. Yu Z., Chen T., Hebert J., Li E., Richard S (2009) **A mouse PRMT1 null allele defines an essential role for arginine methylation in genome maintenance and cell proliferation** *Mol Cell Biol* **29**:2982–2996

54. Guo Z., et al. (2010) **Methylation of FEN1 suppresses nearby phosphorylation and facilitates PCNA binding** *Nat Chem Biol* **6**:766–773

55. He W., et al. (2011) **A role for the arginine methylation of Rad9 in checkpoint control and cellular sensitivity to DNA damage** *Nucleic Acids Res* **39**:4719–4727

56. Yu Z., et al. (2012) **The MRE11 GAR motif regulates DNA double-strand break processing and ATR activation** *Cell Res* **22**:305–320

57. Gurunathan G., Yu Z., Coulombe Y., Masson J.Y., Richard S (2015) **Arginine methylation of hnRNPUL1 regulates interaction with NBS1 and recruitment to sites of DNA damage** *Sci Rep* **5**

58. Clarke T.L., et al. (2017) **PRMT5-Dependent Methylation of the TIP60 Coactivator RUVBL1 Is a Key Regulator of Homologous Recombination** *Mol Cell* **65**:900–916

59. Hamard P.J., et al. (2018) **PRMT5 Regulates DNA Repair by Controlling the Alternative Splicing of Histone-Modifying Enzymes** *Cell Rep* **24**:2643–2657

60. Hellmuth S., Gutierrez-Caballero C., Llano E., Pendas A.M., Stemmann O (2018) **Local activation of mammalian separase in interphase promotes double-strand break repair and prevents oncogenic transformation** *EMBO J* **37**

61. Vadnais C., et al. (2018) **GFI1 facilitates efficient DNA repair by regulating PRMT1 dependent methylation of MRE11 and 53BP1** *Nat Commun* **9**

62. Tan D.Q., et al. (2019) **PRMT5 Modulates Splicing for Genome Integrity and Preserves Proteostasis of Hematopoietic Stem Cells** *Cell Rep* **26**:2316–2328

63. Musiani D., et al. (2020) **PRMT1 Is Recruited via DNA-PK to Chromatin Where It Sustains the Senescence-Associated Secretory Phenotype in Response to Cisplatin** *Cell Rep* **30**:1208–1222

64. Wei X., et al. (2020) **Targeted CRISPR screening identifies PRMT5 as synthetic lethality combinatorial target with gemcitabine in pancreatic cancer cells** *Proc Natl Acad Sci U S A* **117**:28068–28079

65. Sanchez-Bailon M.P., et al. (2021) **Arginine methylation and ubiquitylation crosstalk controls DNA end-resection and homologous recombination repair** *Nat Commun* **12**

66. Giuliani V., et al. (2021) **PRMT1-dependent regulation of RNA metabolism and DNA damage response sustains pancreatic ductal adenocarcinoma** *Nat Commun* **12**

67. Liu L., et al. (2022) **Arginine methylation of BRD4 by PRMT2/4 governs transcription and DNA repair** *Sci Adv* **8**

68. Kim H., et al. (2020) **PRMT5 control of cGAS/STING and NLRC5 pathways defines melanoma response to antitumor immunity** *Sci Transl Med* **12**

69. Wu Q., et al. (2022) **PRMT inhibition induces a viral mimicry response in triple-negative breast cancer** *Nat Chem Biol* **18**:821–830

70. Tang J., et al. (2000) **PRMT1 is the predominant type I protein arginine methyltransferase in mammalian cells** *J Biol Chem* **275**:7723–7730

71. Fuhrmann J., Clancy K.W., Thompson P.R (2015) **Chemical biology of protein arginine modifications in epigenetic regulation** *Chem Rev* **115**:5413–5461

72. Thandapani P., O'Connor T.R., Bailey T.L., Richard S (2013) **Defining the RGG/RG motif** *Mol Cell* **50**:613–623

73. Fedoriw A., et al. (2019) **Anti-tumor Activity of the Type I PRMT Inhibitor, GSK3368715, Synergizes with PRMT5 Inhibition through MTAP Loss** *Cancer Cell* **36**:100–114

74. Gao G., et al. (2019) **PRMT1 loss sensitizes cells to PRMT5 inhibition** *Nucleic Acids Res* **47**:5038–5048

75. Dhar S., et al. (2013) **Loss of the major Type I arginine methyltransferase PRMT1 causes substrate scavenging by other PRMTs** *Sci Rep* **3**

76. Kryukov G.V., et al. (2016) **MTAP deletion confers enhanced dependency on the PRMT5 arginine methyltransferase in cancer cells** *Science* **351**:1214–1218

77. Mavrakis K.J., et al. (2016) **Disordered methionine metabolism in MTAP/CDKN2A-deleted cancers leads to dependence on PRMT5** *Science* **351**:1208–1213

78. Marjon K., et al. (2016) **MTAP Deletions in Cancer Create Vulnerability to Targeting of the MAT2A/PRMT5/RIOK1 Axis** *Cell Rep* **15**:574–587

79. Kalev P., et al. (2021) **MAT2A Inhibition Blocks the Growth of MTAP-Deleted Cancer Cells by Reducing PRMT5-Dependent mRNA Splicing and Inducing DNA Damage** *Cancer Cell* **39**:209–224

80. Metz P.J., et al. (2020) **Symmetric Arginine Dimethylation Is Selectively Required for mRNA Splicing and the Initiation of Type I and Type III Interferon Signaling** *Cell Rep* **30**:1935–1950

81. Siu L.L., et al. (2019) **METEOR-1: A phase I study of GSK3326595, a first-in-class protein arginine methyltransferase 5 (PRMT5) inhibitor, in advanced solid tumours** *Annals of Oncology* **30**

82. Watts J.M., et al. (2019) **A phase I/II study to investigate the safety and clinical activity of the protein arginine methyltransferase 5 inhibitor GSK3326595 in subjects with myelodysplastic syndrome and acute myeloid leukemia** *Blood* **134**

83. Villar M.V., et al. (2020) **537MO First-in-human study of JNJ-64619178, a protein arginine methyltransferase 5 (PRMT5) inhibitor, in patients with advanced cancers** *Annals of Oncology* **31**

84. McKean M., et al. (2021) **Abstract P039: A phase 1 dose escalation study of protein arginine methyltransferase 5 (PRMT5) inhibitor PRT543 in patients with advanced solid tumors and lymphoma** *Molecular Cancer Therapeutics* **20**:P039–P039

85. Falchook G.S., et al. (2021) **Abstract P044: A phase 1 dose escalation study of protein arginine methyltransferase 5 (PRMT5) brain penetrant inhibitor PRT811 in patients with advanced solid tumors, including recurrent high-grade gliomas** *Molecular Cancer Therapeutics* **20**:P044–P044

86. Patel M.R., et al. (2021) **A Phase 1 Dose Escalation Study of Protein Arginine Methyltransferase 5 (PRMT5) Inhibitor PRT543 in Patients with Myeloid Malignancies** *Blood* **138**

87. Rodon Ahnert J., et al. (2021) **Rodon Ahnert, J. et al. (Wolters Kluwer Health, 2021).**

88. Haque T., et al. (2021) **Phase 1 Study of JNJ-64619178, a Protein Arginine Methyltransferase 5 Inhibitor, in Patients with Lower-Risk Myelodysplastic Syndromes** *Blood* **138**

89. Dominici C., et al. (2021) **Synergistic effects of type I PRMT and PARP inhibitors against non-small cell lung cancer cells** *Clin Epigenetics* **13**

90. O'Brien S., et al. (2023) **Inhibiting PRMT5 induces DNA damage and increases anti-proliferative activity of Niraparib, a PARP inhibitor, in models of breast and ovarian cancer** *BMC Cancer* **23**

91. Carter J., et al. (2023) **PRMT5 Inhibitors Regulate DNA Damage Repair Pathways in Cancer Cells and Improve Response to PARP Inhibition and Chemotherapies** *Cancer Res Commun* **3**:2233–2243

92. Li Y., et al. (2023) **PRMT blockade induces defective DNA replication stress response and synergizes with PARP inhibition** *Cell Rep Med* **4**

93. Liberzon A., et al. (2015) **The Molecular Signatures Database (MSigDB) hallmark gene set collection** *Cell Syst* **1**:417–425

94. Knijnenburg T.A., et al. (2018) **Genomic and Molecular Landscape of DNA Damage Repair Deficiency across The Cancer Genome Atlas** *Cell Rep* **23**:239–254

95. Wood R.D., Mitchell M., Sgouros J., Lindahl T (2001) **Human DNA repair genes** *Science* **291**:1284–1289

96. Lord C.J., Ashworth A. (2016) **BRCAness revisited** *Nat Rev Cancer* **16**:110–120

97. Postel-Vinay S., et al. (2013) **A high-throughput screen identifies PARP1/2 inhibitors as a potential therapy for ERCC1-deficient non-small cell lung cancer** *Oncogene* **32**:5377–5387

98. Friboulet L., et al. (2013) **ERCC1 isoform expression and DNA repair in non-small-cell lung cancer** *N Engl J Med* **368**:1101–1110

99. Srour N., Mersaoui S.Y., Richard S (2019) **M-TAP Dance: Targeting PRMT1 and PRMT5 Family Members to Push Cancer Cells Over the Edge** *Cancer Cell* **36**:3–5

100. Rubbi C.P., Milner J (2003) **p53 is a chromatin accessibility factor for nucleotide excision repair of DNA damage** *EMBO J* **22**:975–986

101. Xiang Y., et al. (2017) **RNA m(6)A methylation regulates the ultraviolet-induced DNA damage response** *Nature* **543**:573–576

102. Kwon J., Bakhoum S.F (2020) **The Cytosolic DNA-Sensing cGAS-STING Pathway in Cancer** *Cancer Discov* **10**:26–39

103. Olaussen K.A., et al. (2006) **DNA repair by ERCC1 in non-small-cell lung cancer and cisplatin-based adjuvant chemotherapy** *N Engl J Med* **355**:983–991

104. Lee S.M., et al. (2017) **Randomized Prospective Biomarker Trial of ERCC1 for Comparing Platinum and Nonplatinum Therapy in Advanced Non-Small-Cell Lung Cancer: ERCC1 Trial (ET)** *J Clin Oncol* **35**:402–411

105. Ganzinelli M., et al. (2021) **Single-arm, open label prospective trial to assess prediction of the role of ERCC1/XPF complex in the response of advanced NSCLC patients to platinum-based chemotherapy** *ESMO Open* **6**

106. Chou T.C (2010) **Drug combination studies and their synergy quantification using the Chou-Talalay method** *Cancer Res* **70**:440–446

107. Shen S., et al. (2014) **rMATS: robust and flexible detection of differential alternative splicing from replicate RNA-Seq data** *Proc Natl Acad Sci U S A* **111**:E5593–5601

108. Wang J., Pan Y., Shen S., Lin L., Xing Y (2017) **rMATS-DVR: rMATS discovery of differential variants in RNA** *Bioinformatics* **33**:2216–2217

109. Vivian J., et al. (2017) **Toil enables reproducible, open source, big biomedical data analyses** *Nat Biotechnol* **35**:314–316

110. Mosteller F., Fisher R.A. (1948) **Questions and Answers** *The American Statistician* **2**:30–31

111. Jiang J., et al. (2022) **Systematic illumination of druggable genes in cancer genomes** *Cell Rep* **38**

112. Hu Z., et al. (2021) **The Cancer Surfaceome Atlas integrates genomic, functional and drug response data to identify actionable targets** *Nat Cancer* **2**:1406–1422

113. Hu Z., et al. (2019) **Genomic characterization of genes encoding histone acetylation modulator proteins identifies therapeutic targets for cancer treatment** *Nat Commun* **10**

Editors

Reviewing Editor
Yongliang Yang
Dalian University of Technology, Dalian, China

Senior Editor
Caigang Liu
Shengjing Hospital of China Medical University, Shenyang, China

Reviewer #1 (Public Review):

Summary:

The authors aimed to enhance the effectiveness of PARP inhibitors (PARPi) in treating high-grade serous ovarian cancer (HGSOC) and triple-negative breast cancer (TNBC) by inhibiting PRMT1/5 enzymes. They conducted a drug screen combining PARPi with 74 epigenetic modulators to identify promising combinations.

Zhang et al. reported that protein arginine methyltransferase (PRMT) 1/5 inhibition acts synergistically to enhance the sensitivity of Poly (ADP-ribose) polymerase inhibitors (PARPi) in high-grade serous ovarian cancer (HGSOC) and triple-negative breast cancer (TNBC) cells. The authors are the first to perform a drug screen by combining PARPi with 74 well-characterized epigenetic modulators that target five major classes of epigenetic enzymes. Their drug screen identified both PRMT1/5 inhibitors with high combination and clinical priority scores in PARPi treatment. Notably, PRMT1/5 inhibitors significantly enhance PARPi treatment-induced DNA damage in HR-proficient HGSOC and TNBC cells through enhanced maintenance of gene expression associated with DNA damage repair, BRCAness, and intrinsic innate immune pathways in cancer cells. Additionally, bioinformatic analysis of large-scale genomic and functional profiles from TCGA and DepMap further supports that PRMT1/5 are potential therapeutic targets in oncology, including HGSOC and TNBC. These results provide a strong rationale for the clinical application of a combination of PRMT and PARP inhibitors in patients with HR-proficient ovarian and breast cancer. Thus, this discovery has a high impact on developing novel therapeutic approaches to overcome resistance to PARPi in clinical cancer therapy. The data and presentation in this manuscript are straightforward and reliable.

Strengths:

(1) Innovative Approach: First to screen PARPi with a large panel of epigenetic modulators.
(2) Significant Results: Found that PRMT1/5 inhibitors significantly boost PARPi effectiveness in HR-proficient HGSOC and TNBC cells.
(3) Mechanistic Insights: Showed how PRMT1/5 inhibitors enhance DNA damage repair and immune pathways.
(4) Robust Data: Supported by extensive bioinformatic analysis from large genomic databases.

Weaknesses:

(1) Novelty Clarification: Needs clearer comparison to existing studies showing similar effects.
(2) Unclear Mechanisms: More investigation is needed on how MYC targets correlate with PRMT1/5.
(3) Inconsistent Data: ERCC1 expression results varied across cell lines.
(4) Limited Immune Study: Using immunodeficient mice does not fully explore immune

responses.
(5) Statistical Methods: Should use one-way ANOVA instead of a two-tailed Student's t-test for multiple comparisons.

https://doi.org/10.7554/eLife.99225.1.sa1

Reviewer #2 (Public Review):

Summary:

The authors show that a combination of arginine methyltransferase inhibitors synergize with PARP inhibitors to kill ovarian and triple-negative cancer cell lines in vitro and in vivo using preclinical mouse models.

PARP inhibitors have been the common targeted-therapy options to treat high-grade serous ovarian cancer (HGSOC) and triple-negative breast cancer (TNBC). PRMTs are oncological therapeutic targets and specific inhibitors have been developed. However, due to the insufficiency of PRMTi or PARPi single treatment for HGSOC and TNBC, designing novel combinations of existing inhibitors is necessary. In previous studies, the authors and others developed an "induced PARPi sensitivity by epigenetic modulation" strategy to target resistant tumors. In this study, the authors presented a triple combination of PRMT1i, PRMT5i and PARPi that synergistically kills TNBC cells. A drug screen and RNA-seq analysis were performed to indicate cancer cell growth dependency of PRMT1 and PRMT5, and their CRISPR/Cas9 knockout sensitizes cancer cells to PARPi treatment. It was shown that the cells accumulate DNA damage and have increased caspase 3/7 activity. RNA-seq analysis identified BRCAness genes, and the authors closely studied a top hit ERCC1 as a downregulated DNA damage protein in PRMT inhibitor treatments. ERCC1 is known to be synthetic lethal with PARP inhibitors. Thus, the authors add back ERCC1 and reduce the effects of PRMT inhibitors suggesting PRMT inhibitors mediate, in part, their effect via ERCC1 downregulation. The combination therapy (PRMT/PARP) is validated in 2D cultures of cell lines (OVCAR3, 8 and MDA-MB-231) and has shown to be effective in nude mice with MDA-MB-231 xenograph models.

Strengths and weaknesses:

Overall, the data is well-presented. The experiments are well-performed, convincing, and have the appropriate controls (using inhibitors and genetic deletions) and statistics.

They identify the DNA damage protein ERCC1 to be reduced in expression with PRMT inhibitors. As ERCC1 is known to be synthetic lethal with PARPi, this provides a mechanism for the synergy. They use cell lines only for their study in 2D as well as xenograph models.

https://doi.org/10.7554/eLife.99225.1.sa0